Current Research (2023) Newfoundland and Labrador Department of Industry, Energy and Technology Geological Survey, Report 23-1, pages 47-75

PETROGRAPHY, GEOCHEMISTRY AND GEOCHRONOLOGY OF THE REE-MINERALIZED FOX HARBOUR VOLCANIC BELT, SOUTHEASTERN LABRADOR

Z. Magyarosi and N. Rayner[1]
Mineral Deposits Section
[1]Geolocial Survey of Canada, 601 Booth Street, Ottawa, ON, K1A 0E8

ABSTRACT

The Fox Harbour Volcanic Belt (FHVB) in the Grenville Province of southeastern Labrador is one of several Mesoproterozoic peralkaline complexes hosting rare-earth-element (REE) mineralization, such as the Strange Lake and Flowers River complexes, and the Red Wine Intrusive Suite. The FHVB is ~64 km long, ranging in thickness from 50 m in the east to 3 km in the west, and contains three mineralized belts running parallel to each other. The main rock types are peralkaline volcanic rocks (pantellerite, comendite, and pantelleritic and comenditic trachyte), which host the REE mineralization, non-peralkaline rhyolite and mafic volcanic rocks.

The main minerals in the pantellerite and comendite are quartz, K-feldspar, albite, allanite, magnetite, zircon, titanite and less than 10% biotite and calcic–sodic amphibole and/or pyroxene. Pantelleritic and comenditic trachyte are composed of albite, ~30% calcic–sodic pyroxene and amphibole, biotite, K-feldspar, zircon and allanite. The REE minerals identified in this study include allanite, fergusonite, locally REE-titanite, rare britholite and two unidentified phases. They crystallized late and occur with zircon, magnetite, titanite, local apatite and mafic minerals.

Geochronology of four samples from the Deep Fox deposit in the eastern part of the FHVB indicate that the rocks crystallized ca. *1300 Ma and were subjected to Grenvillian metamorphism* ca. *1050 Ma. Non-peralkaline rhyolite returned an igneous crystallization age of 1269 ± 9.5 Ma overprinted by a metamorphic age of 1031 ± 15 Ma. Comendite returned an igneous crystallization age of 1314 ± 12 Ma and pantellerite returned a metamorphic age of 1065 ± 8.2 Ma. A sample from a leucogabbro located north of the FHVB returned an igneous crystallization age of* ca. *1300 Ma overprinted by a metamorphic age of 1038 ± 29 Ma.*

The FHVB is bimodal. The felsic rocks are peralkaline to metaluminous, A-type rhyolites and trachytes. Mineralization is hosted in the most strongly fractionated rocks characterized by the highest REE, high-field-strength element (HFSE: Zr, Hf, U, Th) and Fe contents, with the Zr content up to 26 361 ppm. The light-rare-earth element (LREE) and heavy-rare-earth element (HREE) enrichments are 100 to 20 000 times higher and 10 to 1000 times higher than the chondrite concentrations, respectively. The east FHVB (EFHVB) has higher concentrations of LREEs than the west FHVB (WFHVB), similar concentrations of HREEs, but the HREE/LREE ratio is higher in the WFHVB. Parts of the FHVB underwent Na loss and K metasomatism resulting in their apparent metaluminous nature.

The results of this study highlight the complex evolution (magmatic, hydrothermal and metamorphic) of the FHVB and associated REE mineralization and challenges some aspects of the current models for this type of deposit, such as the lack of significant REE mineralization in peralkaline extrusive rocks and the increase in degree of fractionation over time.

INTRODUCTION

This report summarizes the petrography, geochemistry and geochronology of the Fox Harbour Volcanic Belt (FHVB), host to rare-earth-element (REE) mineralization in the Port Hope Simpson–St. Lewis area, southeastern Labrador. It is part of a multi-year project, funded by the Geological Survey of Newfoundland and Labrador (GSNL) and the Geological Survey of Canada (GSC) through its Targeted Geoscience Initiative (TGI) program, and is being undertaken in collaboration with Search Minerals Incorporated. The purpose of the project is to advance the understanding of the genesis of REE mineralization hosted in peralkaline rocks.

The FHVB is a *ca.* 1.3 Ga peralkaline complex, similar in age to other REE-mineralized Mesoproterozoic peralkaline complexes in Labrador including the Strange Lake and Flowers River complexes as well as the Red Wine Intrusive Suite (Miller *et al.*, 1997; Crocker, 2014; Ducharme *et al.*, 2021). These deposits are enriched in both heavy-rare-earth elements (HREE) and light-rare-earth elements (LREE) and may be more beneficial for REE mining and processing compared to the REE deposits hosted in ionic clays and carbonatites. The latter are relatively enriched in the less-valuable LREE, and the ionic clays are enriched in HREE, but they are typically very low grade and have a lower recovery rate (Dostal, 2016; Goode, 2021).

In the Port Hope Simpson–St. Lewis area, REE mineralization was discovered by Search Minerals Incorporated in 2010. It is currently in an advanced stage of exploration, but the genesis of the mineralization remains uncertain. Although REE mineralization also occurs south of the FHVB, in the Pinware terrane, this report concentrates on three occurrences along the FHVB; namely the Deep Fox and Foxtrot in the eastern Fox Harbour Volcanic Belt (EFHVB), and the Fox Meadow in the western Fox Harbour Volcanic Belt (WFHVB; Figures 1 and 2). The report includes new data on whole-rock geochemistry, petrography, Scanning Electron Microscope (SEM) analyses, Scanning Electron Microscope-Mineral Liberation Analysis (SEM-MLA), and geochronology of selected samples.

REE MINERALIZATION IN PERALKALINE IGNEOUS SYSTEMS

Peralkaline rocks are characterized by having a peralkaline index (molar (Na+K)/Al) larger than 1, resulting in the presence of minerals with excess alkalies, such as sodic amphiboles and pyroxenes. They occur in igneous systems also containing a variety of other alkaline, metaluminous, and mafic rocks (Beard *et al.*, 2022). Peralkaline silicic volcanic systems, such as the FHVB, are commonly bimodal, characterized by mafic–felsic volcanism with an absence of rocks of intermediate compositions (52–62 wt. %; MacDonald, 2012). The rocks include peralkaline rhyolites and trachytes, subdivided into pantellerite, comendite, and pantelleritic and comenditic trachytes, based on their FeO_{total} and Al_2O_3 contents (MacDonald, 1974). The more evolved pantellerite and pantelleritic trachyte have higher FeO_{total} and lower Al_2O_3 contents than comendite and comenditic trachyte. Peralkaline rocks evolve toward an "effective minima composition" (EMC) of FeO_{total} ~13 wt. % and Al_2O_3 ~5 wt. %, peralkaline index ~3 and SiO_2 content between 64 and 69 wt. %, which leads to increasing concentrations of REEs, high-field-strength elements (HFSE) and volatiles (Linnen and Keppler, 1997, 2002; MacDonald, 2012).

Rare-earth-element mineralization in peralkaline igneous systems is the result of a combination of magmatic and late-magmatic hydrothermal processes (Beard *et al.*, 2022). The magmatic processes include low-degree, high-pressure partial melting of a metasomatized mantle source beneath a thick continental crust, followed by protracted fractional crystallization in a magma chamber resulting in an enrichment of incompatible elements, such as REEs, HFSE and volatiles. Protracted fractional crystallization is enabled by the abundance of volatiles, which typically include F, Cl and C (carbohydrates or CO_2). Late-magmatic hydrothermal fluids, formed by volatiles exsolving from the cooling magma, remobilize the REEs and, in some cases, enrich the primary REE mineralization.

REGIONAL GEOLOGY

The Grenville Province in eastern Labrador is composed of late Paleoproterozoic to Mesoproterozoic rocks formed *via* multiple orogenic and related events including the Eagle River orogenesis (1810–1775 Ma), Labradorian orogenesis (1710–1600 Ma), Pinwarian orogenesis (1520–1460 Ma), post-Pinwarian–pre-Grenvillian events (1460–1090), Grenvillian orogenesis (1090–920 Ma), and Neoproterozoic and Phanerozoic events (Gower, 2019). It is subdivided into five terranes, namely, from north to south: the Groswater Bay, Lake Melville, Hawke River, Mealy Mountains and Pinware terranes (Figure 1; Gower, 2019). The FHVB is located in the Mealy Mountains terrane, straddling the boundary with the Lake Melville terrane to the north. The terranes are distinguished from one another based on the type and degree of deformation and metamorphism they underwent during each orogenic event. The Mealy Mountains terrane is distinguished from the Pinware terrane by the presence of significant pre-Pinwarian history. The Lake Melville terrane went through severe Grenvillian deformation, whereas the Mealy Mountains and Pinware terranes were only moderately affected by Grenville orogenesis (Gower, 2019).

The Mealy Mountains terrane is underlain by late Paleoproterozoic rocks and minor amounts of Mesoproterozoic rocks (Gower, 2019; van Nostrand, 1992; van Nostrand *et al.*, 1992; Nunn and van Nostrand, 1996a, b; Figure 1). The oldest units are pre-Labradorian crustal rocks (1810–1770 Ma) consisting of metasedimentary, mostly pelitic gneisses (P3sgn), and minor granitoid rocks of the Eagle River Complex (undivided P3gdn). Early Labradorian rocks (1710–1660 Ma) include granitoids (P3gm and P3gdn), which comprise the most widespread units in the Mealy Mountains terrane, and minor anorthositic, mafic and ultramafic rocks of the Upper Eagle River mafic intrusion (undivided P3gdn). Late Labradorian

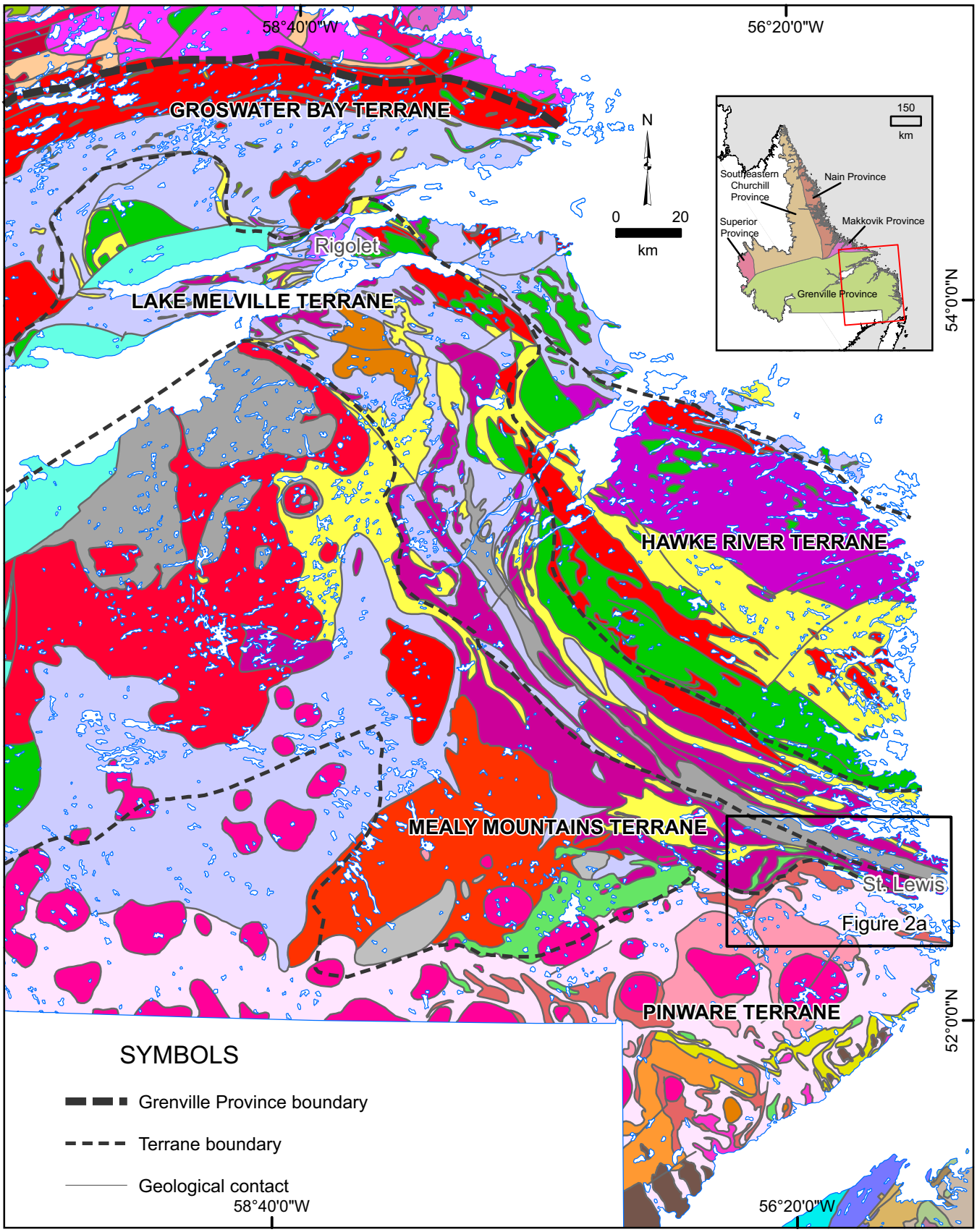

Figure 1. *Simplified geology map of the Grenville Province in eastern Labrador (Wardle* et al.*, 1997).*

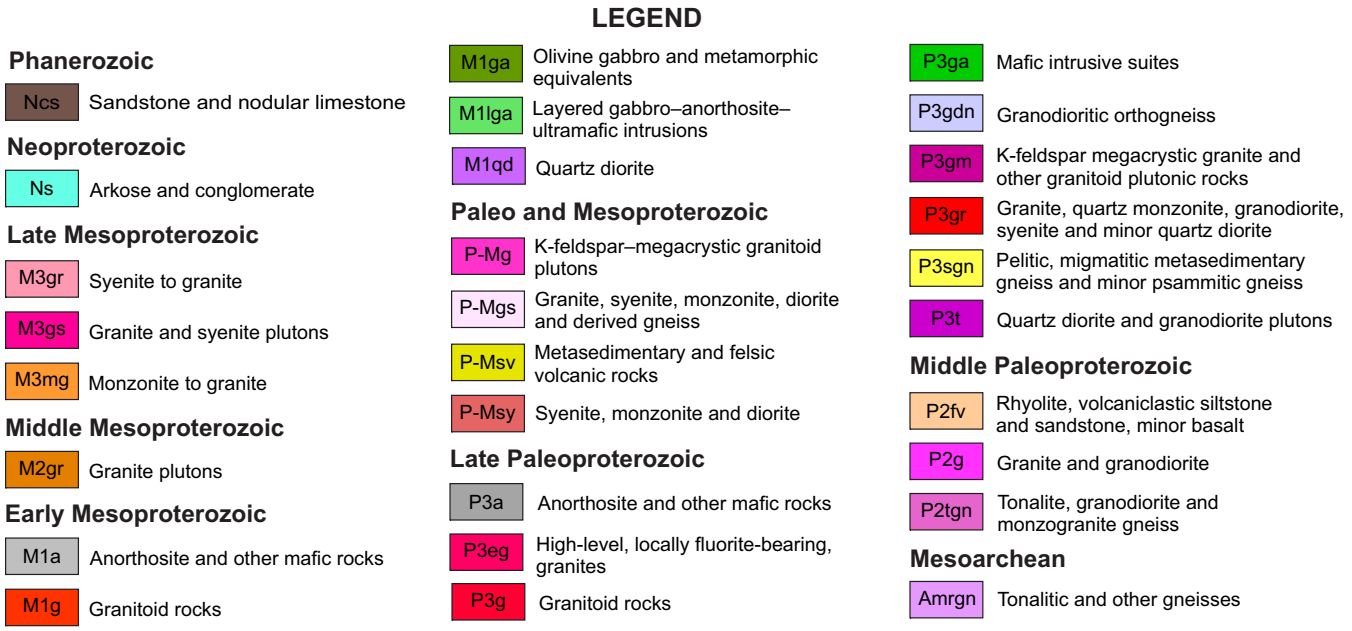

Figure 1. *Legend.*

rocks (1660–1600 Ma) consist of mafic, anorthositic and felsic rocks of the Mealy Mountains Intrusive Suite (MMIS), which is a typical anorthosite–monzonite/mangerite–charnockite–granite (AMCG) complex (P3a and P3g), and granitoids of the Middle Eagle River pluton (P3gr). Early Mesoproterozoic rocks (1600–1350 Ma) include the Pinware–Mealy Mountains terrane boundary mafic and anorthositic rocks (M1a and M1lga) and anorthositic to felsic rocks of the Upper Paradise River Intrusive Suite (M1g). Middle Mesoproterozoic rocks (1350–1200 Ma) include the bimodal FHVB and the Mealy diabase dykes.

The eastern Mealy Mountains terrane is structurally attenuated, reduced from approximately 80 km maximum width in the west, to approximately 5 km wide within the eastern structural wedge (Figures 1 and 2A; Gower, 2019). This attenuation is the result of northwest–southeast compression during the Grenville orogeny and is accommodated by northeast-striking, southeast-verging thrusts/reverse faults and strike–slip faults in the St. Lewis River area, west of the FHVB. Structures in the eastern wedge of the Mealy Mountains terrane suggest dextral-oblique-slip, northeast-side-up motion along the Fox Harbour Fault, which separates the Mealy Mountains and Lake Melville terranes (Figure 2A). The boundary between the Mealy Mountains terrane and the Pinware terrane is marked by the Long Harbour Fault that passes through the St. Lewis Inlet. A pressure–temperature estimate ~8 km southwest of the Fox Meadow occurrence (Figure 2A) yielded a temperature of 800°C and a pressure of 8 kbars (Gower, 2019). Haley (2014) indicated that the rocks of the FHVB underwent amphibolite-facies metamorphism during Grenville orogenesis, based on the observed mineral assemblages and zircon growth at ~1.05 Ga.

LOCAL GEOLOGY

The FHVB is located mostly in the eastern structural wedge of the Mealy Mountains terrane (Gower, 2019; Figure 2A, B). The most common rock types in EFHVB area are foliated to gneissic megacrystic, porphyritic granitoid rocks or augen gneiss, followed by a gneissic granodiorite. Minor amphibolite lenses and layers occurring within the gneisses are interpreted as remnants of dykes. Mafic rocks are more common toward the west. At the Fox Meadow occurrence in the WFHVB, the dominant rock types include gneissic anorthosite, gabbro and norite.

FOX HARBOUR VOLCANIC BELT

The FHVB is subdivided into three mineralized belts running parallel to each other, namely, from north to south: the Road Belt, the Magnetite Belt and the South Belt (Figure 2B; Haley, 2014; Miller, 2015). The Road Belt extends throughout the entire length the FHVB, whereas the Magnetite and South belts only occur in the eastern half. The age of the rocks separating the three mineralized belts is uncertain. According to Gower (2019), these rocks are older, based on the similarities to the rocks occurring in the Mealy Mountains and Lake Melville terranes to the west and north of the FHVB. Miller (2015) interpreted these rocks to be part of the FHVB and renamed the three mineralized belts and the rocks separating them as Fox Harbour domain.

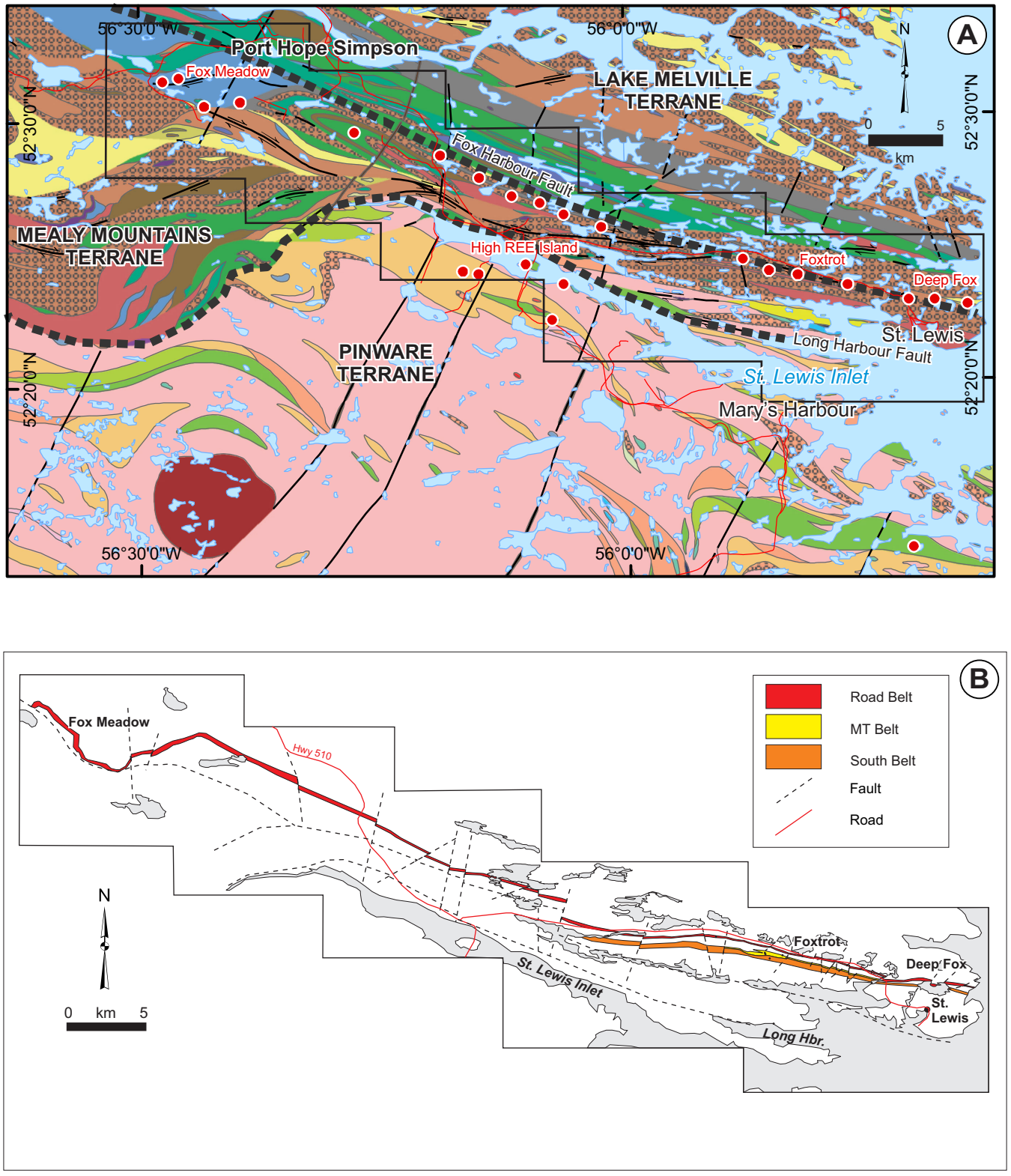

Figure 2. *A) Geology of the Port Hope Simpson area (after Gower, 2010a, b, 2019); B) The Fox Harbour Volcanic Belt (after Gower, 2019).*

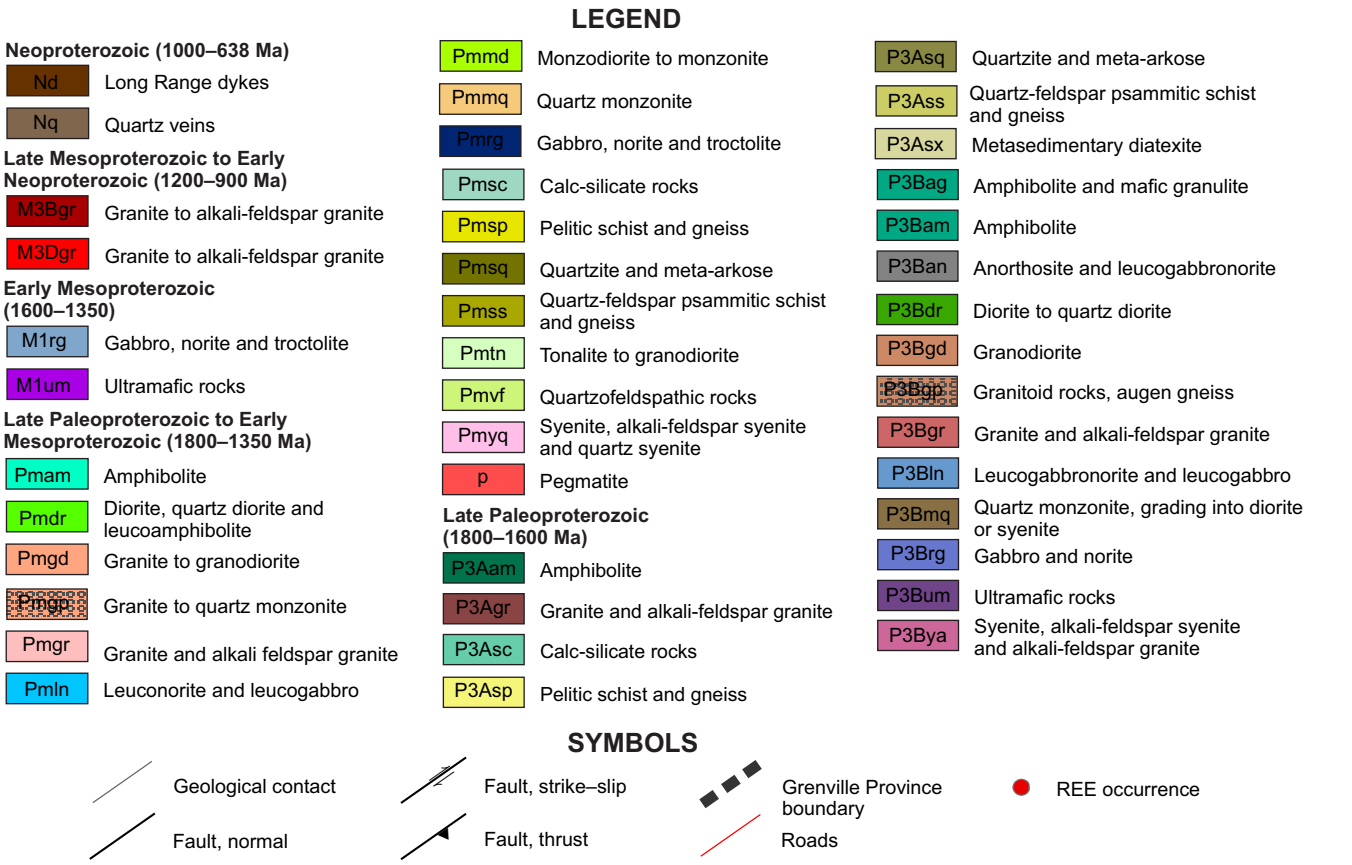

Figure 2. *Legend.*

The FHVB is a mylonitized and metamorphosed bimodal volcanic belt composed of quartz-oversaturated peralkaline volcanic rocks (pantellerite to comendite and pantelleritic to comenditic trachytes), non-peralkaline rhyolite and mafic volcanic rocks, along with minor volcaniclastic sedimentary rocks and quartzite (Haley, 2014; Miller, 2015). Based on the presence of mafic units with the felsic rocks, metasedimentary rocks interpreted as volcaniclastic, and large epidote pods in the mafic rocks interpreted as altered pillows or alteration pipes, previous workers concluded that the protoliths are volcanic (Haley, 2014; Miller, 2015; Gower, 2019). Pantellerite in the FHVB typically contains significant amounts of magnetite, locally occurring as phenocrysts, and zircon. Based on the amount of Zr, pantellerite is subdivided into Zr-poor pantellerite (5000 to 10 000 ppm Zr), pantellerite (10 000 to 15 000 ppm Zr) and Zr-rich pantellerite (more than 15 000 ppm Zr; Miller, 2015).

MINERALIZATION

Mineralization is hosted in pantellerite to pantelleritic trachyte, occurring mostly in the Road Belt (*e.g.*, Deep Fox, Fox Meadow deposits) and Magnetite Belt (*e.g.*, Foxtrot deposit), and comendite to comenditic trachyte, occurring in all three belts. In the EFHVB, zirconium-rich pantellerite and pantellerite host all of the medium- to high-grade mineralization, characterized by Dy concentrations between 100 and 300 ppm. Comendite hosts low-grade mineralization with Dy concentrations between 20 and 100 ppm. Most of the REEs are hosted in allanite and fergusonite, where allanite contains mostly LREE, and fergusonite contains HREE and minor LREE. Additional REE minerals include chevkinite, bastnaesite, synchysite, monazite and rare columbite (Haley, 2014; Masun *et al.*, 2016; Ciuculescu *et al.*, 2022). The resources at Deep Fox and Foxtrot were recently updated by Ciuculescu *et al.* (2022) and are summarized in Table 1.

Table 1. Resources at the Deep Fox and Foxtrot deposits (Ciuculescu *et al.*, 2022)

Deposit	Resource type	Total resource (Mt)	Pr (ppm)	Nd (ppm)	Dy (ppm)	Tb (ppm)
Deep Fox	Indicated	5.1	394	1469	202	34
Deep Fox	Inferred	3.3	366	1381	198	33
Foxtrot	Indicated	10	366	1368	176	30
Foxtrot	Inferred	3	371	1384	177	30

ANALYTICAL METHODS

A total of 186 samples were collected in the summer of 2021 from the Deep Fox (53 samples), Foxtrot (87 samples) and Fox Meadow (46 samples) occurrences. Whole-rock geochemical analyses were completed at the geochemical laboratory of the Geological Survey of Newfoundland and Labrador (GSNL). Samples were cleaned, crushed, pulverized and analyzed according to Finch *et al.* (2018). Polished thin sections of representative samples were examined using a petrographic microscope.

Four samples from Deep Fox, two samples from Foxtrot and four samples from Fox Meadow containing the highest concentrations of REEs were selected for analysis using a FEI MLA 650FEG SEM at Memorial University of Newfoundland (MUN) Micro Analysis Facility (MUN MAFIIC). Qualitative analyses were completed using high throughput Energy-dispersive X-ray Spectroscopy (EDX) detectors from Bruker (https://www.mun.ca/creait/). A subset of five samples were chosen for SEM-MLA analysis to determine the abundances of minerals in the samples. The SEM-MLA uses backscattered electron imaging (BEI) to measure the average atomic number of the minerals to establish grain boundaries, then classifies the grains as minerals using a mineral reference list and allows quantitative evaluation of the abundances of minerals, among other characteristics.

Geochronological analyses of four samples from the Deep Fox area were undertaken at the Geological Survey of Canada in Ottawa. All samples were disaggregated using standard crushing/pulverizing techniques followed by density separation using the Wilfley table and heavy liquids, followed by magnetic separation (unless otherwise noted). For SHRIMP analysis, selected grains were cast in epoxy mounts (IP1005 and 1013). The mid-sections of the minerals were exposed through polishing using a diamond compound, and internal features characterized in back-scattered electron mode (BSE) utilizing a Zeiss Evo 50 scanning electron microscope. Mount surfaces were evaporatively coated with 10 nm of high-purity Au. SHRIMP analytical procedures followed those described by Stern (1997). Fragments of the Temora2 primary zircon reference material (RM) GSC lab number 10493 ($^{206}Pb/^{238}U$ age = 416.5 ± 0.22 Ma, Black *et al.*, 2004) and secondary zircon RMs 6266 ($^{206}Pb/^{238}U$ age = 559 ± 02 Ma, Stern and Amelin, 2003) 1242 ($^{207}Pb/^{206}Pb$ age = 2679.7 ± 0.2 Ma, Davis *et al.*, 2019) and 9910 (441.2 ± 0.4 Ma, B. Davis and V. McNicoll, 2010, unpublished data) were analyzed on the same mount and under the same conditions as the unknowns. Analyses were conducted using an O− primary beam, with a spot size of either 16 or 12 µm at a beam current between 3−6 nA. The count rates of the isotopes of Hf, U, Th and Pb as well as Hf and Yb for zircon were sequentially measured over six scans with a single electron multiplier. Off-line data processing was accomplished using Squid3 (Bodorkos *et al.*, 2020) software. Decay constants used follow the recommendations of Steiger and Jäger (1977). The 1σ external errors of $^{206}Pb/^{238}U$ ratios reported in the data table (Appendix A) incorporate a ± 0.8–1.2 error in calibrating the primary RM (*see* Stern and Amelin, 2003). Analyses of a secondary zircon RM 1242 were interspersed between the sample analyses to assess the requirement of an isotopic mass fractionation correction for the $^{207}Pb/^{206}Pb$ age, however none was required. Details of the analytical session (mount/session number, spot size, and primary beam intensity) are recorded in the footnotes of the data table as is the measured weighted mean age for the secondary RMs for that session (Appendix A). Common Pb correction utilized the Pb composition of the surface blank (Stern, 1997). Isoplot v. 4.15 (Ludwig, 2012) was used to generate concordia plots and calculate weighted means. The error ellipses on the concordia diagrams, and the weighted mean errors are reported at 95% confidence, unless otherwise noted. In the text and relevant figures, U–Pb dates are reported as 2σ error limits, unless otherwise noted. Errors reported in the data table (Appendix A) are given at the 1σ confidence interval.

RESULTS

PETROGRAPHY

East Fox Harbour Volcanic Belt: Deep Fox and Foxtrot

The main rock types at Deep Fox and Foxtrot include pantellerite, comendite, non-peralkaline rhyolite and basalt. All rocks are foliated, folded and intruded by pegmatite lenses up to 3 m thick. The list of minerals, modal mineralogy and MLA maps of three representative pantellerite samples are shown in Table 2 and Plate 1. The main minerals in the pantellerite are quartz, K-feldspar, albite, allanite, magnetite, zircon, and less than 10% biotite, amphibole and/or pyroxene, and locally calcite. Accessory minerals include titanite, apatite, fluorite, chlorite and the rest of the REE minerals, which are fergusonite, Y-allanite, britholite and two unidentified minerals. All samples display compositional layering defined by various proportions of magnetite, ferromagnesian minerals, calcite, allanite and/or feldspars (Plate 1). The modal proportion of ferromagnesian minerals is higher at Foxtrot than at Deep Fox. The amphibole and pyroxene are calcic–sodic. Locally, pyroxene and amphibole are intergrown, with one replacing the other, but the order of crystallization is uncertain (Plate 2A). Titanite commonly occurs surrounding magnetite (Plate 2B). Rare-earth-element minerals typically form aggregates and occur with zircon, apatite, magnetite, titanite and mafic minerals, if present (Plate 2C, D). The composition of allanite varies based on the relative REE, Ca and Fe contents (Plate 2D).

Table 2. Results of the SEM-MLA modal analyses. Rare-earth-element minerals are highlighted in red

Sample number	019A01	079A01	039A05	059B01	060A02
Area	Deep Fox	Deep Fox	Foxtrot	Fox Meadow	Fox Meadow
Quartz	55.02	61.77	44.16	0.40	8.78
Orthoclase	25.13	5.86	14.67	2.53	8.00
Allanite	6.25	6.24	3.11	1.75	2.15
Albite	3.43	10.60	21.35	58.68	12.14
Magnetite	3.15	5.82	3.66	0.02	0.05
Calcite	2.22		0.51		0.01
Zircon	2.01	1.79	1.49	2.74	2.30
Titanite	0.89	0.80	1.25	0.67	0.23
Pyroxene	0.52	0.01	9.07	23.73	41.07
Y-Allanite	0.39		0.16		0.08
Apatite	0.20	0.68	0.10		0.01
Biotite	0.24	3.79	0.08	7.54	2.94
Chlorite	0.13	0.02	0.01	0.10	0.03
Fergusonite	0.23	0.16	0.20	0.07	0.10
Amphibole	0.08	1.79	0.08	1.54	18.92
Britholite	0.06		0.03		0.74
Spessartine	0.01	0.05			
Thorite	0.01		0.01		
Muscovite	0.01	0.01			
Fluorite		0.33			0.13
Sphalerite			0.02		
Y-Si-Ca-LREE		0.09		0.04	
Y-Si-Fe-Ca-REE		0.13		0.04	
Titanite-REE				0.01	2.31
Ilmenite				0.06	0.01

Fergusonite most commonly occurs with zircon, and locally contains inclusions of galena (Plate 2E). The unidentified REE minerals are silicates containing Y and LREE, Ca and locally Fe, with one grain containing Pb (Plate 2F). The mineralogy and textural relationships in comendite are the same as in the pantellerite, but it contains less magnetite, zircon, titanite and REE minerals. Amphibole is partially replaced by biotite in some of the comendite samples (Plate 2G, H).

The minerals in the non-peralkaline rhyolite include quartz, K-feldspar, albite, biotite, epidote and less common amphibole, muscovite, apatite, zircon, chlorite, titanite, fluorite and allanite. It is uncertain whether the epidote is primary or secondary. In one sample, amphibole is surrounded by biotite and epidote (Plate 3A, B). Chlorite forms as an alteration after biotite. Allanite typically occurs in the centre of epidote (Plate 3C, D). As illustrated in Plate 3E, F displaying the boundary between a pantellerite and non-peralkaline rhyolite, the non-peralkaline rhyolite contains more K-feldspar and epidote, less magnetite, zircon, titanite and REE minerals compared to pantellerite.

The main minerals in the mafic rocks include plagioclase, amphibole, clinopyroxene, biotite, titanite, apatite, chlorite, allanite, ilmenite and epidote (Plate 3G, H). Amphibole has a yellow-green to blue-green pleochroism and may be zoned. Pyroxene is colourless with a 2nd order birefringence consistent with augite.

West Fox Harbour Volcanic Belt: Fox Meadow

The rock types at Fox Meadow include pantelleritic and comenditic trachyte, pantellerite, comendite and basalt. They are all foliated, folded and cut by pegmatite lenses and dykes of several generations. The boundary between pantellerite and pantelleritic trachyte appears to be gradational and is difficult to determine due to subtle changes not visible at the hand sample scale. Pantellerite is similar to the pantellerite at Deep Fox and Foxtrot, therefore it will not be described here in detail.

The list of minerals and modal mineralogy from a representative pantelleritic trachyte sample from Fox Meadow (059B01) is shown in Table 2. Plate 4 shows the MLA maps of two samples from Fox Meadow. Sample 060A02 contains a mafic clast and it is not representative (Table 2 and Plate 4, sample 060A02). The main minerals in pantelleritic trachyte are albite, pyroxene, amphibole, biotite, K-feldspar, zircon and allanite. Accessory minerals include quartz, ilmenite or magnetite, titanite, chlorite, fluorite and the rest of the REE minerals, which are fergusonite, Y-allanite, REE-rich titanite, britholite and the same unidentified silicates as at Deep Fox. The rocks are medium grained and there is less compositional layering observed at thin-section scale than at the Foxtrot and Deep Fox deposits (Plate 4, sample 059B01). The amount of ferromagnesian minerals is ~30%, which is significantly more than in pantellerite (Table 2). Locally, it contains mafic clasts consisting of mostly pyroxene (~50%), amphibole, biotite and quartz (Plate 4, samples 060A02 and 355A02). The mafic clasts typically occur within pegmatites and their mineralogy differs from the basalt interlayered with the pantelleritic trachyte.

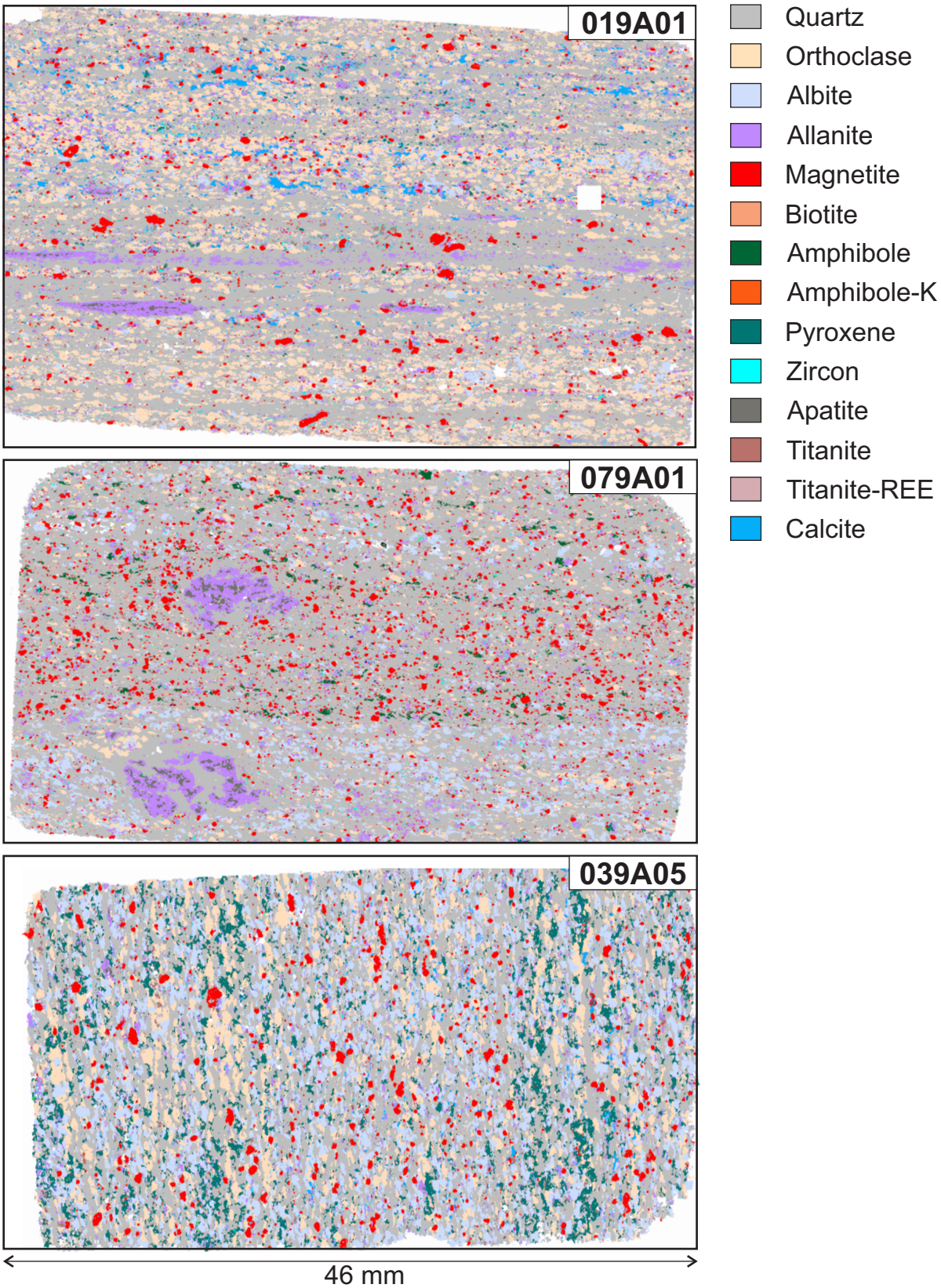

Plate 1. *X-ray maps of two samples from Deep Fox (019A01 and 079A01) and one sample from Foxtrot (039A05).*

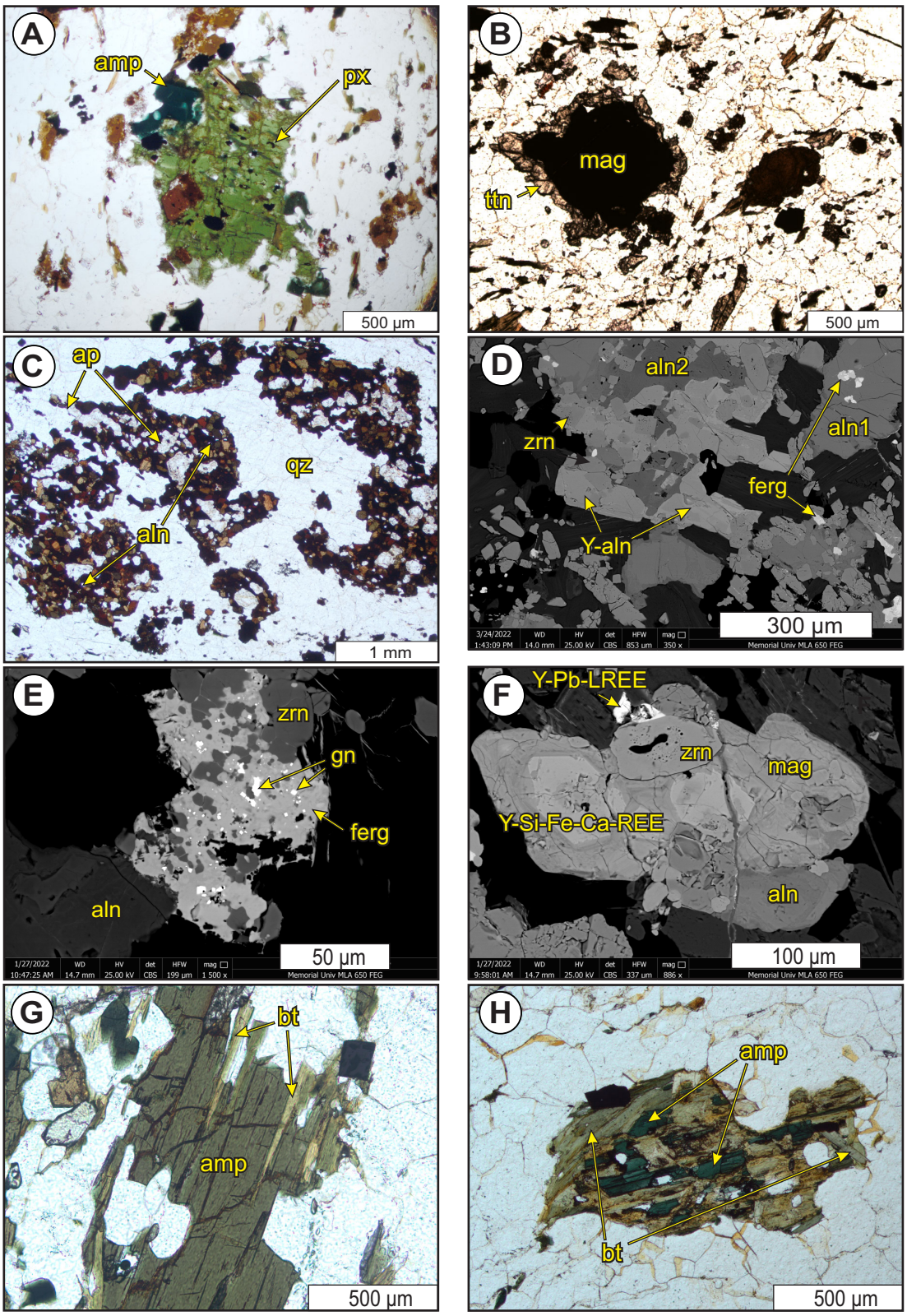

Plate 2. *Representative photomicrographs and back-scattered electron (BSE) images of pantellerite and comendite from Deep Fox and Foxtrot. A) Pyroxene and amphibole; B) Magnetite surrounded by titanite; C) Allanite forming aggregates with apatite; D) BSE image of allanite, fergusonite and zircon. Note the change in the composition of allanite (aln1, aln2 and Y-aln); E) BSE image of fergusonite and zircon. Fergusonite contains inclusions of galena; F) BSE image of unidentified REE-silicate containing Fe, Ca, Y and REEs, and locally Pb; G) Amphibole partially replaced by biotite along cleavages in comendite; H) Amphibole partially altered to biotite in comendite. Mineral abbreviations on all plates are according to Whitney (2010).*

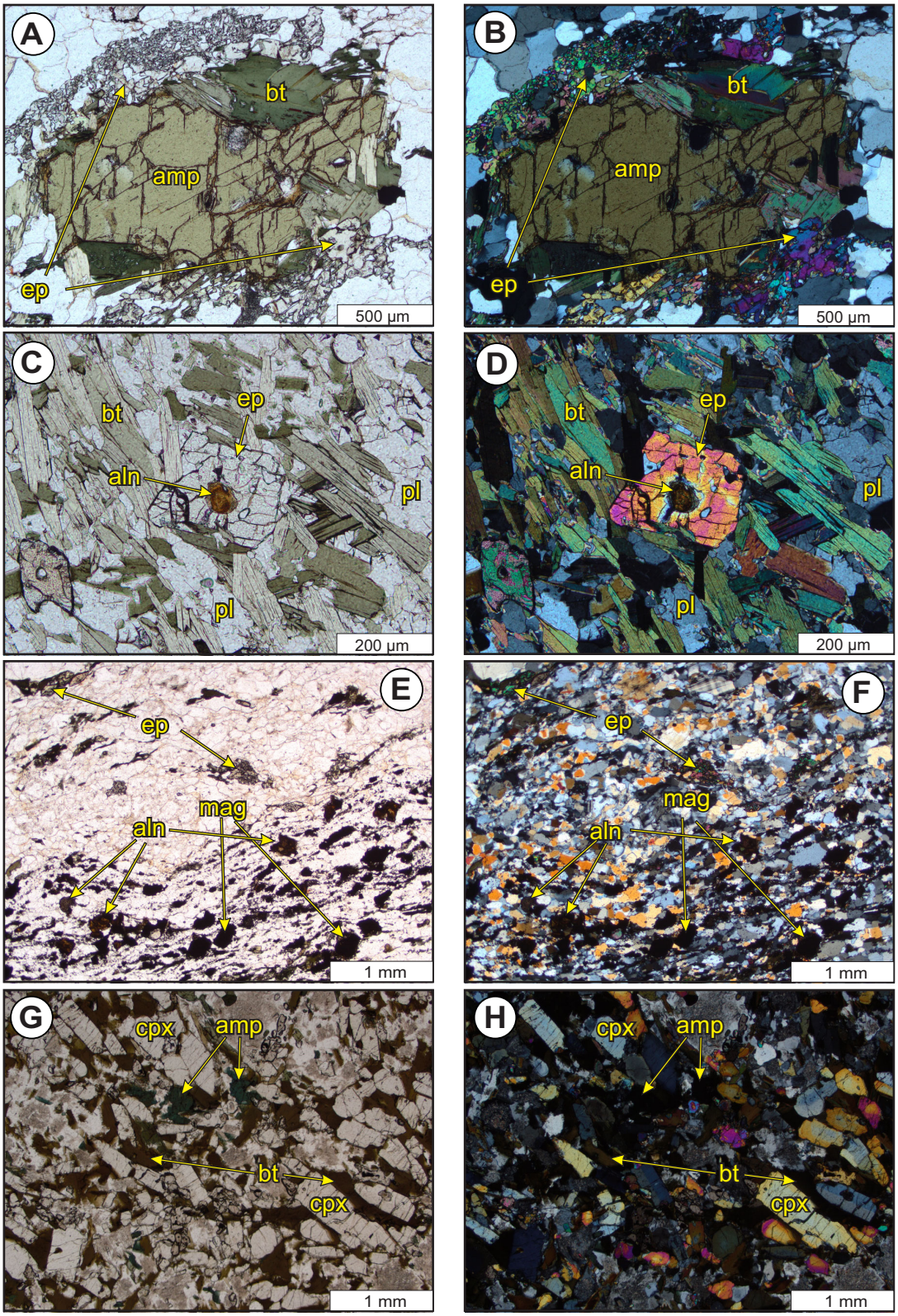

Plate 3. *Representative photomicrographs of non-peralkaline rhyolite and basalt from Deep Fox and Foxtrot. A) Amphibole surrounded by biotite and epidote; B) Same as A under crossed polars; C) Allanite in the centre of epidote; D) Same as C under crossed polars; E) Boundary of non-peralkaline rhyolite (top) and pantellerite (bottom); F) Same as E under crossed polars; G) Basalt containing clinopyroxene, amphibole and biotite; H) Same as G under crossed polars.*

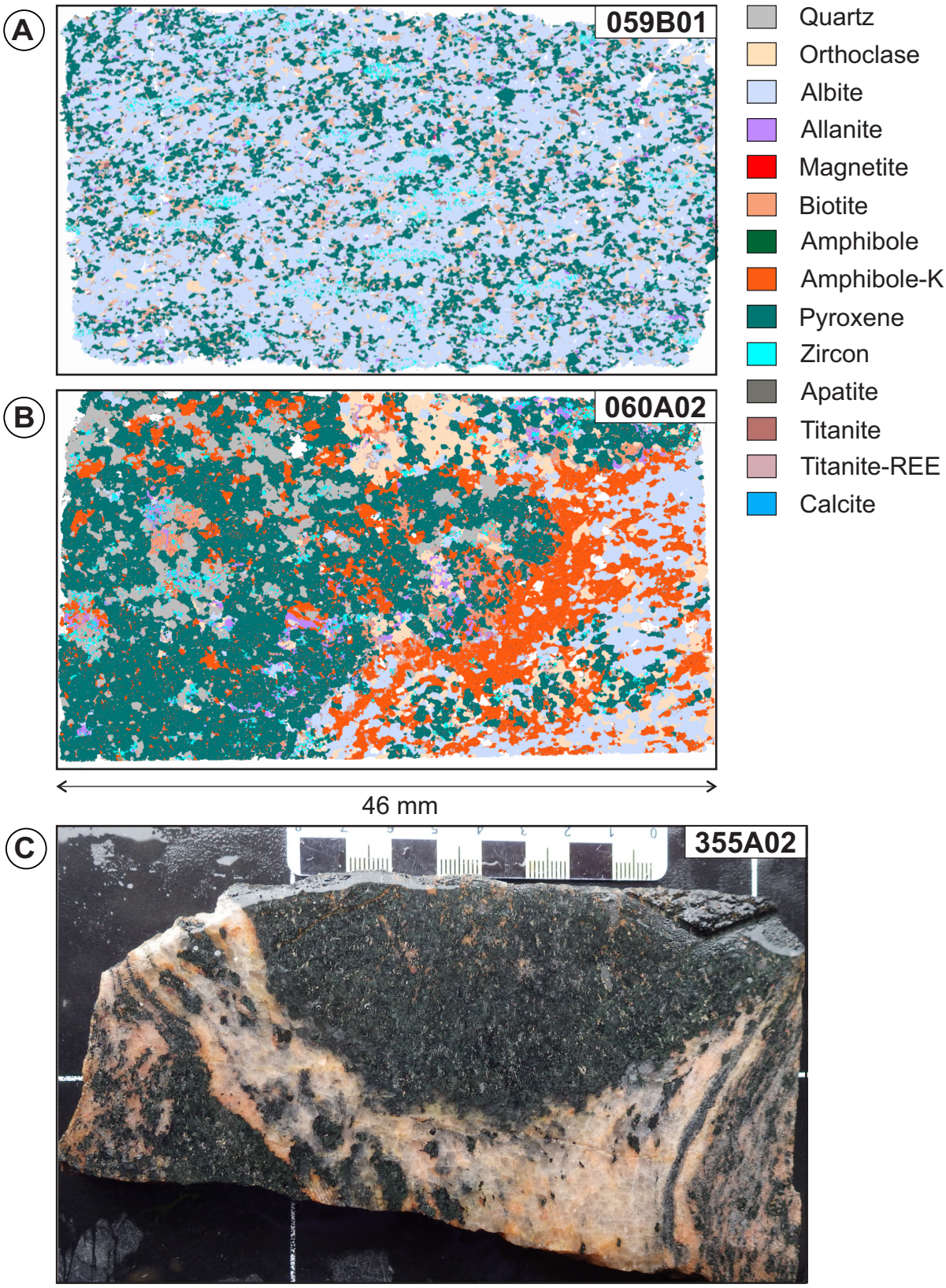

Plate 4. *A) X-ray map of a representative pantelleritic trachyte sample (059B01) from Fox Meadow; B) X-ray map of Fox Meadow sample (060A02) containing mafic clast; C) Polished slab (355A02) from Fox Meadow containing mafic clast in pegmatite.*

Based on their optical properties and SEM analysis, the pyroxene and amphibole are calcic–sodic (Plate 5A). They are locally intergrown, similar to the EFHVB, suggesting that one partially replaced the other, but the order of crystallization is also uncertain. The biotite is dark brown to black due to inclusions of REE minerals (Plate 5B, C). Allanite mostly occurs as disseminated grains with other REE minerals and zircon (Plate 5D), and along the cleavage planes of biotite (Plate 5C, E), suggesting that it formed later than biotite. Locally, it occurs as veins in silicates (Plate 5F). Similar to the EFHVB, the composition of allanite changes, with darker and brighter varieties observed under the SEM (Plate 5D). Fergusonite typically occurs with zircon and allanite, commonly along the grain boundaries of zircon (Plate 5G). Rare-earth-element-rich titanite occurs with allanite, locally being surrounded by it, indicating that it crystallized before allanite (Plate 5H). Rare britholite occurs around the edges of allanite (Plate 5D).

The mafic rocks at Fox Meadow are composed of amphibole, biotite, plagioclase, titanite, local pyroxene, trace apatite and minor to trace amounts of quartz and opaque minerals including ilmenite, pyrite and chalcopyrite. Ilmenite is typically surrounded by titanite, similar to the felsic rocks. Plagioclase is locally partially saussuritized.

GEOCHRONOLOGY

Previous geochronology studies using U–Pb in zircon from rhyolitic units in the FHVB have indicated a crystallization age of *ca.* 1.3 Ga within all three belts around the Foxtrot deposit, and a Grenvillian age of metamorphism of *ca.* 1.05 Ga (Haley, 2014). All samples selected for geochronology are from the Deep Fox area. They include a mineralized pantellerite (21ZM065A01), a comendite (21ZM084A01), a non-peralkaline rhyolite (21ZM081A01) and a sample from a leucogabbro unit (21ZM176A01) bordering the Road Belt to the north (Plate 6). The results of the geochronology are summarized in Table 3.

Sample 21ZM065A01 (GSC Lab Number 12706)

Sample 21ZM065A01 is a light-pink to grey, fine- to medium-grained, foliated, strongly magnetic pantellerite (Plate 6). It contains thin (<0.5 cm) felsic layers and pegmatites composed of quartz and K-feldspar. Minerals include quartz, K-feldspar, albite, magnetite, zircon, titanite, biotite, amphibole, pyroxene, REE minerals and fluorite.

An abundant zircon separate was recovered consisting of clear, colourless prismatic grains (aspect ratio generally 2:1, 3:1). In plane light, some grains have a high density of inclusions forming an inner cloudy "core". In CL imagery, the zoning is quite unusual. Whereas zoning in zircon is generally concentric, the zoning observed in this sample appears to be highly disrupted, or in some cases patchy (Figure 3A). This does not seem to correspond with inclusions, where it might be expected that regular zoning is disrupted when wrapping around inclusions.

The $^{206}Pb/^{238}U$ results from 37 analyses of 34 separate zircon grains range from 913 to 1238 Ma and fall on a chord toward the origin of the concordia diagram (Figure 3B). This scatter both above and below concordia, on a chord to the origin, is likely the result of an analytical artifact related to variable U–Pb fractionation behaviour both between grains in this sample and relative to the fractionation behaviour of the zircon reference material related to the crystallographic matrix of the zircon. The unusual zoning pattern of these zircons might also be a reflection of an atypical zircon matrix. The $^{207}Pb/^{206}Pb$ age determined by SHRIMP is not affected by these matrix effects and thus will be used to interpret these results. The weighted mean $^{207}Pb/^{206}Pb$ age of 33 of these analyses is 1065.9 ± 8.2 Ma (MSWD = 1.5, probability of fit = 0.048). This excludes one older analysis from a core with distinctive, regular oscillatory zoning as well as the three youngest analyses. Based on the previous geochronology in the area, this age is interpreted as a metamorphic age, which is also consistent with its low Th/U (typically 0.1). No primary igneous zircon was identified in this sample, although the one excluded older analysis of 1238 Ma might reflect an igneous core.

Sample 21ZM084A01 (GSC Lab Number 12709)

This sample is a foliated pink to grey, medium-grained, homogeneous and equigranular, magnetic comendite (Plate 6). The minerals include quartz, K-feldspar, albite, biotite, magnetite, titanite, amphibole, zircon, REE minerals, apatite, trace amounts of calcite and fluorite and locally garnet. Amphibole is locally surrounded by biotite (Plate 2G, H). Allanite occurs with magnetite and zircon.

An abundant zircon separate consists of clear, colourless prismatic grains (aspect ratio generally 2:1, 3:1). In CL, these are characterized by a good CL response (relatively moderate to low U content) exhibiting broad sector zoning (Figure 3C). Sixteen analyses were carried out on 16 separate grains, which yielded a single statistical population with a weighted mean $^{206}Pb/^{238}U$ age of 1314 ± 12 Ma (MSWD = 0.52, probability of fit = 0.93, Figure 3D). This is interpreted as the igneous crystallization age of the comendite. No metamorphic zircon was identified.

Sample 21ZM081A01 (GSC Lab Number 12710)

The sample is a foliated pink to grey, fine-grained, homogeneous and equigranular, weakly magnetic non-per-

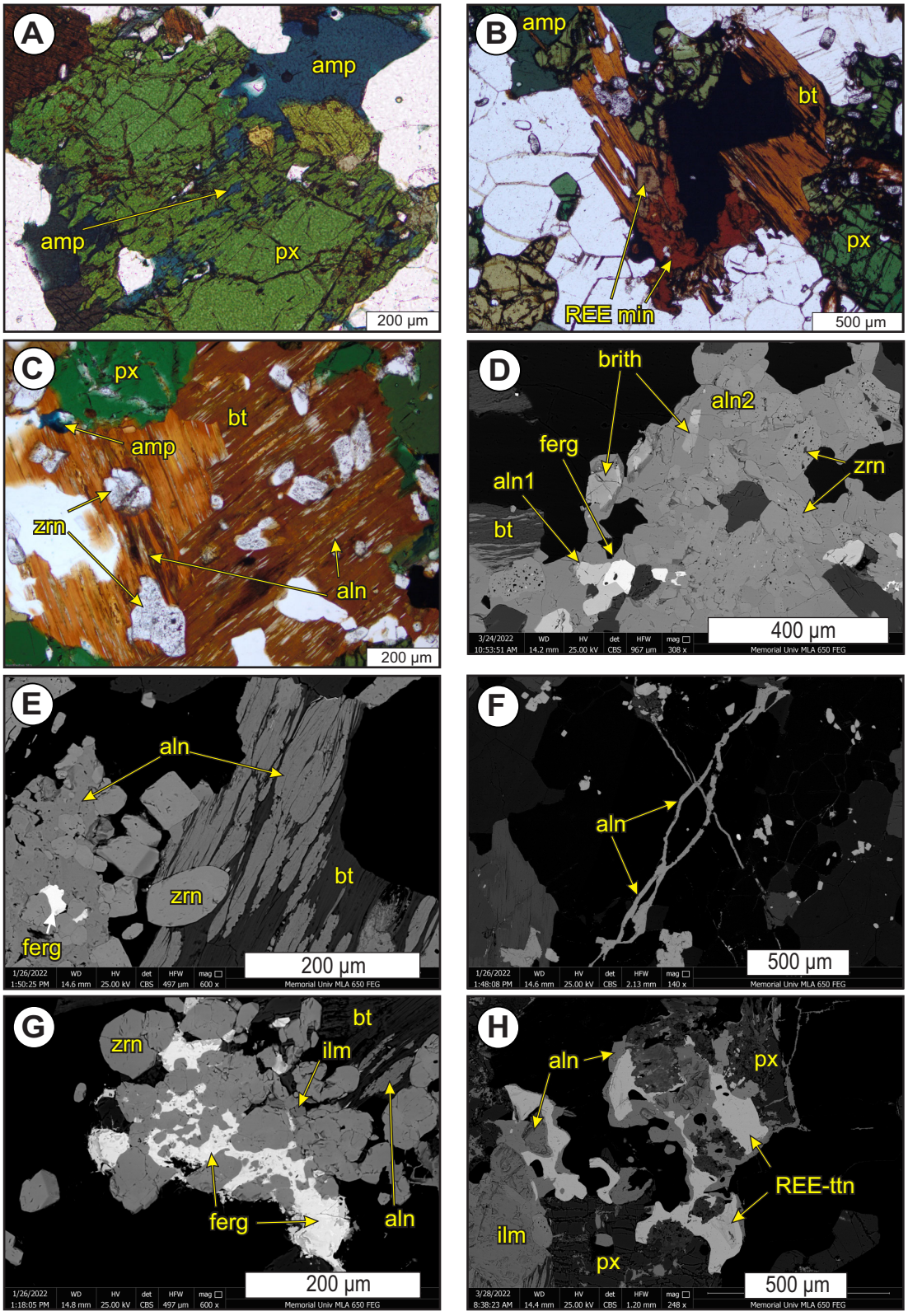

Plate 5. *Representative photomicrographs and BSE images from Fox Meadow: A) Intergrown amphibole and pyroxene; B) Biotite containing REE minerals; C) Allanite along the cleavage planes of biotite; D) BSE image of allanite of variable composition (aln1 and aln2), fergusonite, britholite and zircon; E) BSE image of allanite along the cleavage planes of biotite; F) Allanite vein in silicates; G) Fergusonite around the grain boundaries of zircon; H) BSE image of REE-rich titanite surrounded by allanite.*

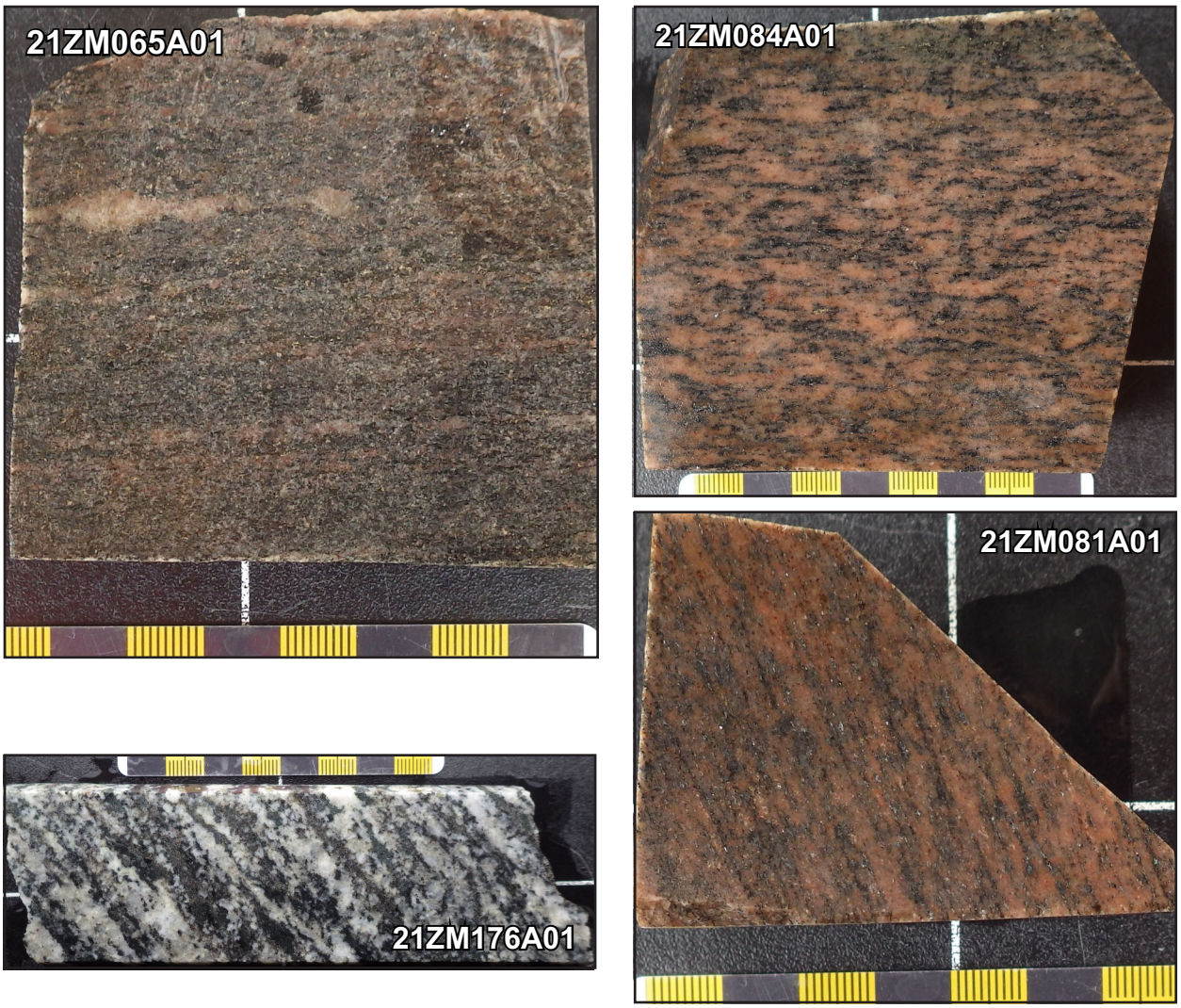

Plate 6. *Slabs of samples selected for geochronology. The scale is in centimetres.*

Table 3. *Summary of the results of the geochronology analyses*

Sample number	Lab number	Lithology	Age	Interpretation
21ZM065A01	12706	Pantellerite	1065.9 ± 8.2 Ma	Metamorphism
21ZM084A01	12709	Comendite	1314 ± 12 Ma	Igneous crystallization
21ZM081A01	12710	Non-peralkaline rhyolite	1269.0 ± 9.5 Ma	Igneous crystallization
21ZM081A01	12710	Non-peralkaline rhyolite	1031 ± 15 Ma	Metamorphism
21ZM176A01	12707	Leucogabbro	*ca.* 1300 Ma	Igneous crystallization
21ZM176A01	12707	Leucogabbro	1038 ± 29 Ma	Metamorphism

alkaline rhyolite (Plate 6). It consists of quartz, K-feldspar, albite, muscovite, zircon and trace amounts of magnetite and/or ilmenite, biotite, allanite and apatite. Allanite is rare and it occurs with zircon, but also surrounded by epidote. Amphibole is surrounded by muscovite around a pegmatite vein.

An abundant zircon separate was collected consisting of euhedral, prismatic, colourless to pale pink/brown zircon grains that contain abundant inclusions, both opaque and transparent. Many grains are also highly fractured. The zircons from this sample are characterized by concentric zoning in CL images (Figure 3E). Many grains have dark CL

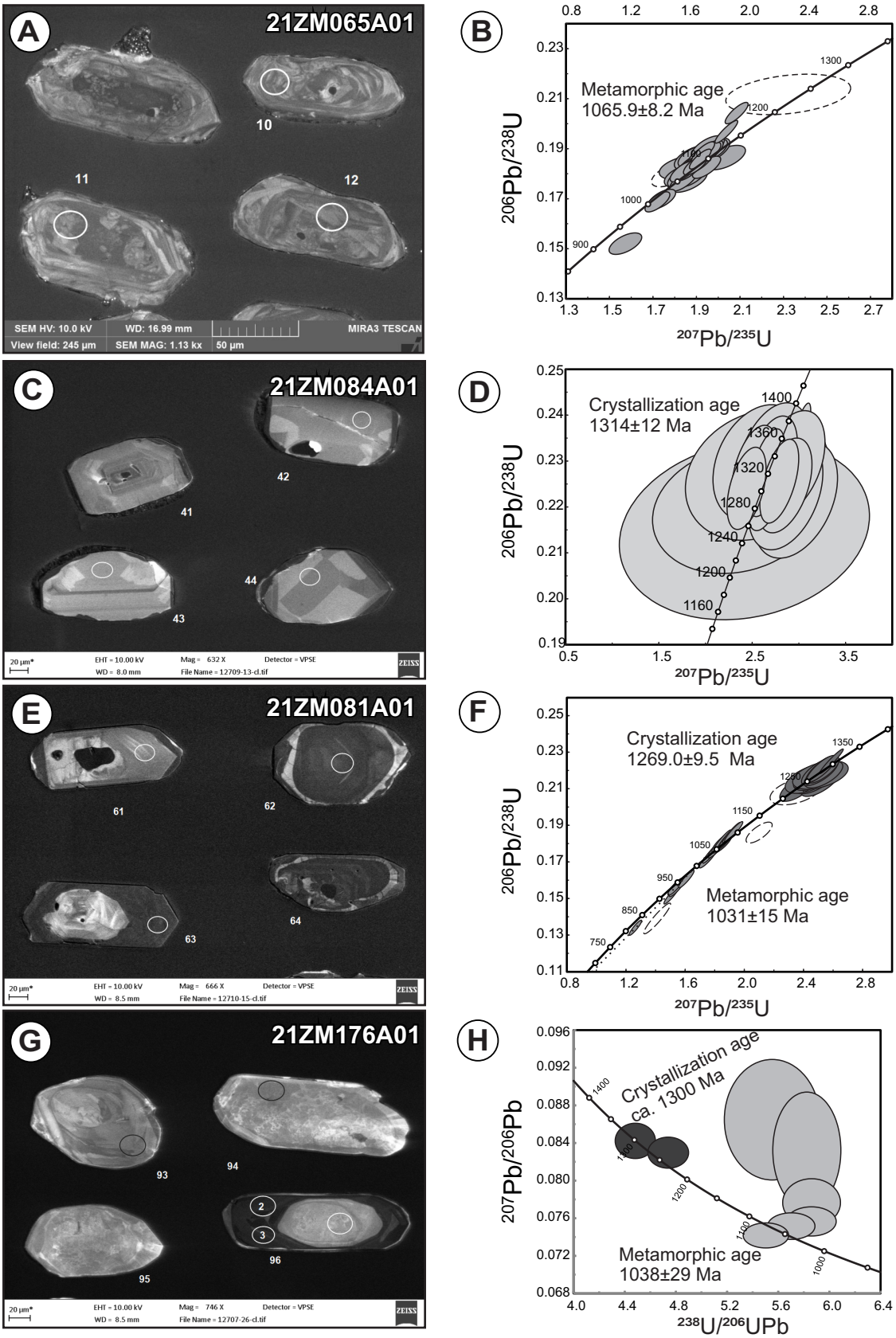

Figure 3. *Cathodoluminescence (CL) images of zircons and concordia diagrams of the geochronology samples from the Deep Fox area, A, B) Pantellerite; C, D) Comendite; E, F) Non-peralkaline rhyolite; G, H) Leucogabbro.*

(high U) overgrowths, some of these overgrowths are concordant with the zoning in the interior of the grain, whereas in other cases the boundary with the core transgresses the zoning.

Thirty-five analyses were carried out on 28 separate zircon grains. Analyses from cores/inner parts of concentrically zoned grains have consistently high Th/U (0.6–1.5) and yield a weighted mean $^{206}Pb/^{238}U$ age of 1269.0 ± 9.5 Ma (n=17, MSWD = 1.4, probability = 0.12), which is interpreted as the igneous crystallization age of the non-peralkaline rhyolite. Three younger analyses from cores were excluded, two of which are highly discordant (Figure 3F). Fifteen rims were also analyzed. These consistently have low Th/U (<0.06) and plot along a discordia chord. A regression through this chord yields an upper intercept of 1031 ± 15 Ma, which is interpreted as the age of a metamorphic overprint. The lower intercept of the regression is 573 ± 65 Ma (MSWD = 1.00), but the geological significance of this age is unknown.

Sample 21ZM176A01 (GSC Lab Number 12707)

The sample is a foliated white to dark-grey with minor dark-green, medium- to coarse-grained leucogabbro (Plate 6). This gabbro unit is located north of the Road Belt and stretches through the whole length of the FHVB. The composition of the gabbro varies from anorthosite to melanogabbro. Minerals include amphibole (10 to 75%), plagioclase (50 to 90%), biotite, ilmenite, titanite, epidote, chlorite and trace amounts of quartz, pyrite and chalcopyrite. Plagioclase is locally altered to saussurite.

Abundant zircons were recovered from this sample. These are clear, colourless prismatic grains (aspect ratio generally 2:1, 3:1). The majority of the zircon grains have very strong CL response indicating very low U concentrations. This was confirmed during SHRIMP analysis with the majority of the grains having less than 3 ppm U, making them impractical for age determinations. The grains with the darkest CL response (highest U) were further analyzed (Figure 3G). These yielded results with between 14–241 ppm U. The two oldest analyses (1235 and 1301 Ma) are from the interior parts of grains that are also characterized by a Th/U of *ca.* 0.9. The remaining 6 analyses, all of which contain less than 1 ppm Th (and thus extremely low Th/U), yield a weighted mean $^{206}Pb/^{238}U$ age 1038 ± 29 Ma (MSWD = 3.5, probability = 0.004). Whereas the dataset for this sample is extremely limited, it suggests that the crystallization age of the leucogabbro is *ca.* 1.3 Ga (the age of the oldest analysis with high Th/U), which was metamorphosed at *ca.* 1030 Ma (Figure 3H).

GEOCHEMISTRY

The FHVB is bimodal, consisting of mafic and felsic rocks with no intermediate compositions (Figure 4A; Pearce, 1996). The felsic rocks form a trend from rhyolite–dacite to alkali rhyolite, with most of them falling in the alkali rhyolite field. Felsic rocks from Deep Fox plot in 3 groups, representing pantellerite, comendite and non-peralkaline rhyolite, from top to bottom. Felsic rocks from Fox Meadow plot mostly with the pantellerites, on the top of the trend. Foxtrot felsic rocks form a continuous trend through the whole range of felsic rocks, which may be due to fine interlayering of the different rock types. The mafic rocks fall in the basalt field (Figure 4A). On the Al_2O_3 *vs.* FeO_{total} diagram (MacDonald, 1974), most of the felsic rocks plot in the pantellerite field, with some in the pantelleritic trachyte and comendite field, and a few in the comenditic trachyte field (Figure 4B). The most evolved sample contains 17.00 wt. % FeO_{total} and 6.13 wt. % Al_2O_3.

Most felsic rocks fall in the A-type granite field, forming three distinct groups representing pantellerite and pantelleritic trachyte, comendite and non-peralkaline rhyolite, from the top right corner to the lower left part of the Zr *vs.* 10^4 Ga/Al diagram (Figure 4C; Whalen *et al.*, 1987). The few samples not plotting in the A-type granite field contain muscovite, which is not common in peralkaline complexes, suggesting that they are most likely not part of FHVB or muscovite is an alteration mineral. Most felsic rocks fall in the within-plate granite (WPG) field forming a trend with the most evolved rocks also plotting in the upper right corner of the diagram (Figure 4D; Pearce *et al.*, 1984; Christiansen and Keith, 1996; Förster *et al.*, 1997).

On Shand's (1922) diagram, the felsic rocks range from peralkaline to peraluminous (Figure 5). Most of the Fox Meadow samples are peralkaline, in agreement with the presence of abundant sodic–calcic pyroxene and amphibole. The Deep Fox samples range from metaluminous to peraluminous and the Foxtrot samples show the whole range of peralkaline to peraluminous compositions. A few of the examined samples contain muscovite, which is consistent with their peraluminous nature, although some of them may not be part of the FHVB, also suggested by these samples plotting outside of the A-type granite field, or muscovite may be secondary. Most of the Deep Fox samples contain biotite and only trace amounts of sodic pyroxene and amphibole in agreement with its metaluminous nature. In order to examine the effects of alteration, the samples were plotted on the diagrams of Hughes (1973), and Spitz and Darling (1978). Some of the felsic rocks from mostly Deep Fox and Foxtrot, including all pantellerites, were affected by K-metasomatism and Na-loss (Figure 6). A few samples from all three areas show the effects of Na-metasomatism.

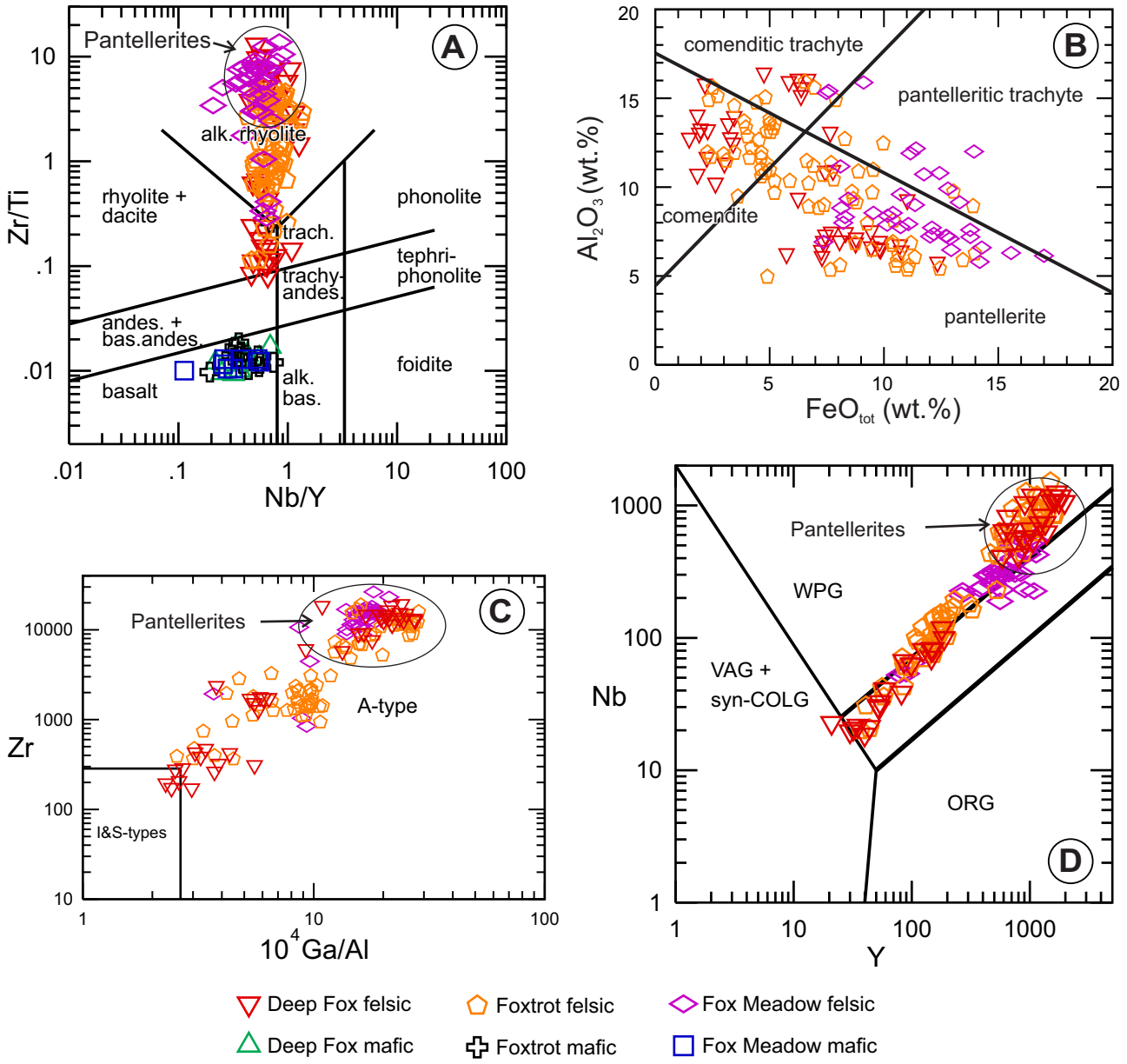

Figure 4. *Chemical classification and tectonic discrimination of the FHVB. A) Zr/Ti* vs. *Nb/Y rock classification (Pearce, 1996); B) Al_2O_3* vs. *FeO_{total} classification of peralkaline volcanic rocks (MacDonald, 1974); C) Zr* vs. *10^4Ga/Al (Whalen* et al.*, 1987); D) Nb vs. Y (Pearce* et al.*, 1984; Christiansen and Keith, 1996; Förster* et al.*, 1997).*

There is a strong positive correlation between Zr and Hf with the Zr content ranging between 53 and 26 361 ppm and the Hf content ranging between 1.4 and 663 ppm (Figure 7A). The Zr/Hf ratio is between ~20 and ~50 and shows a positive correlation with Hf until ~100 ppm Hf, after which it becomes nearly constant around 40 in the most evolved rocks (Figure 7B). The Nb/Ta ratio varies between ~10 and ~40 showing no correlation with Ta (Figure 7C). Thorium concentrations range up to 670 ppm, and U concentrations range up to 107.3 ppm, with the Th/U ratio ranging between 0.9 and 26.70 ppm and an average of 5.35 ppm (Figure 7D); suggesting that most of the FHVB is "high-heat producing" (HHP) (Sharma *et al.*, 2019). The F content of the felsic rocks ranges up to 7346 ppm with an average of 1159 ppm.

Most of the FHVB plots outside of the OIB field on the Yb/Ta *vs.* Y/Nb diagram, indicating that the FHVB is mostly an A2-type granite (Figure 8A; Eby, 1992). The Y/Nb ratio ranges between 0.74 and 8.85 with an average of 1.82, and the Yb/Ta ratio ranges between 1.73 and 14.80 with an average of 3.50. On ternary diagrams from Eby (1992), most of the samples plot along the boundary between the A1 and

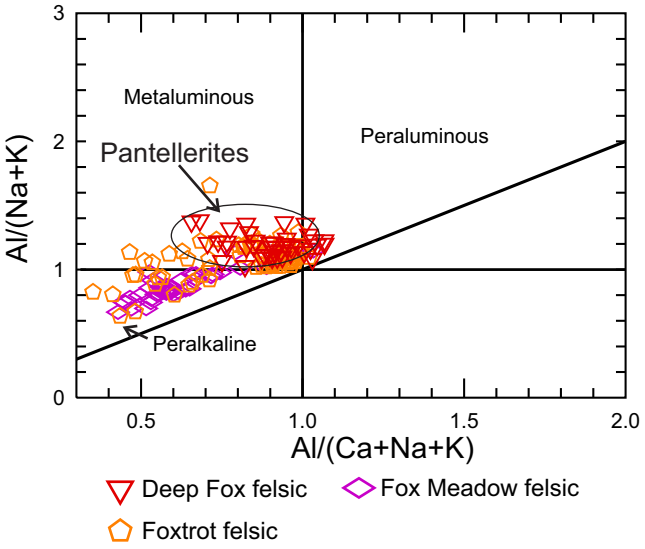

Figure 5. *Al/(Na+K) molar ratio* vs. *aluminum-saturation index (Shand, 1922).*

A2 granites, although on the Y-Nb-3*Ga ternary diagram, most of the Fox Meadow rocks plot in the A2 field, and only some of the Deep Fox and Foxtrot samples plot in the A1 field (Figure 8B, C).

On chondrite-normalized spider diagrams, the REEs form negative slopes from La to Lu for both felsic and mafic rocks (Figure 9). The LREE and HREE enrichments in felsic rocks is 100 to 20 000 times and 10 to 1000 times higher than the chondrite concentrations, respectively. The REE pattern in most of the felsic rocks from Fox Meadow becomes flat after Dy (Figure 9G), contrary to the Deep Fox and Foxtrot felsic rocks (Figure 9C, E). All felsic rocks are characterized with a deep negative Eu anomaly. The REE enrichment in the mafic rocks ranges between 8 and 200 times the chondrite values. On extended primitive-mantle normalized trace-element plots, the felsic rocks are characterized by negative Cs, Ba, K, Pb, Sr, P and Ti anomalies, most of which are likely due to fractional crystallization of various minerals including feldspars and possibly ilmenite (Figure 9B, D, F, H). The mafic rocks display positive Rb, K, Pb and Eu anomalies and negative Th, U and Nb anomalies. On the Lu *vs.* La diagram (Figure 10), the slope defined by the Fox Meadow samples is steeper than that at Deep Fox and Foxtrot, suggesting a relative increase in Lu compared to La at Fox Meadow. The amount of LREE is higher at Deep Fox and Foxtrot than at Fox Meadow, but the amount of HREE is similar and the HREE/LREE ratio is higher at Fox Meadow (Figure 10). This is consistent with the flattening of the HREE slope in the Fox Meadow samples on the chondrite-normalized REE pattern (Figure 9G).

DISCUSSION

ROCK TYPES

The FHVB is a bimodal, peralkaline complex as suggested by the presence of interlayered felsic and mafic rocks, the lack of rocks with intermediate compositions, and the presence of calcic–sodic amphibole and pyroxene (Beard *et al.*, 2022). The compositional layering observed in all felsic rocks is most likely primary igneous, due to the variable compositions of the layers, most of which are not

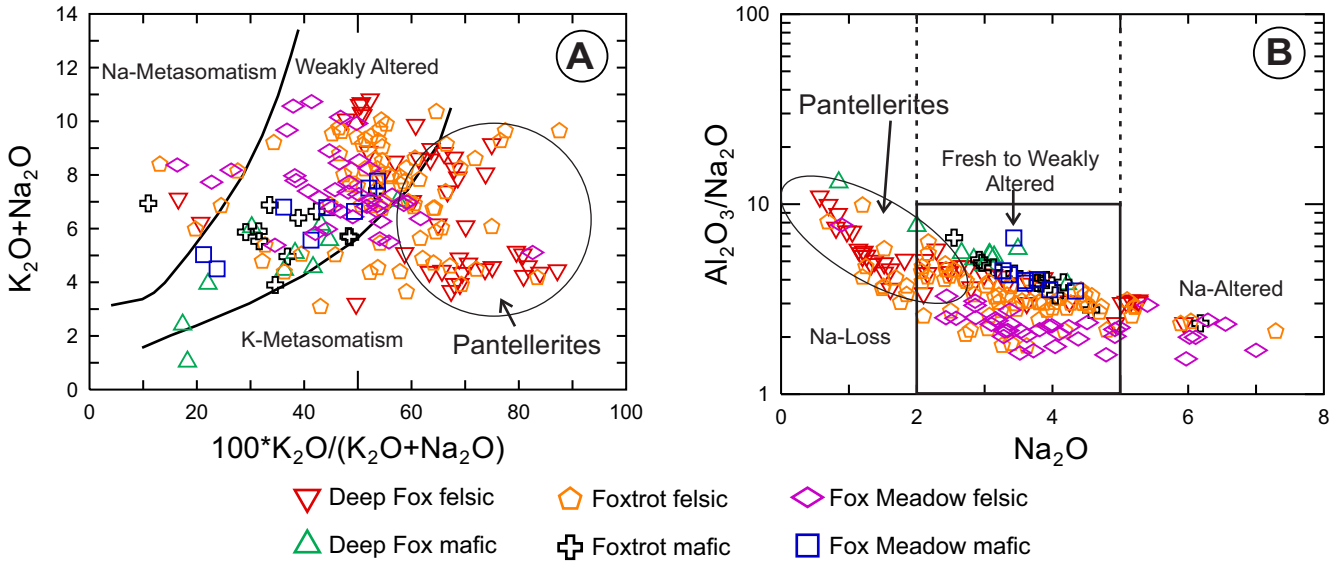

Figure 6. *Diagrams showing the effects of alteration and/or metamorphism. A) Hughes (1973) diagram separating weakly altered, and K- and Na-metasomatized rocks; B) Spitz and Darling (1978) diagram separating fresh to weakly altered rocks from rocks affected by Na loss or gain.*

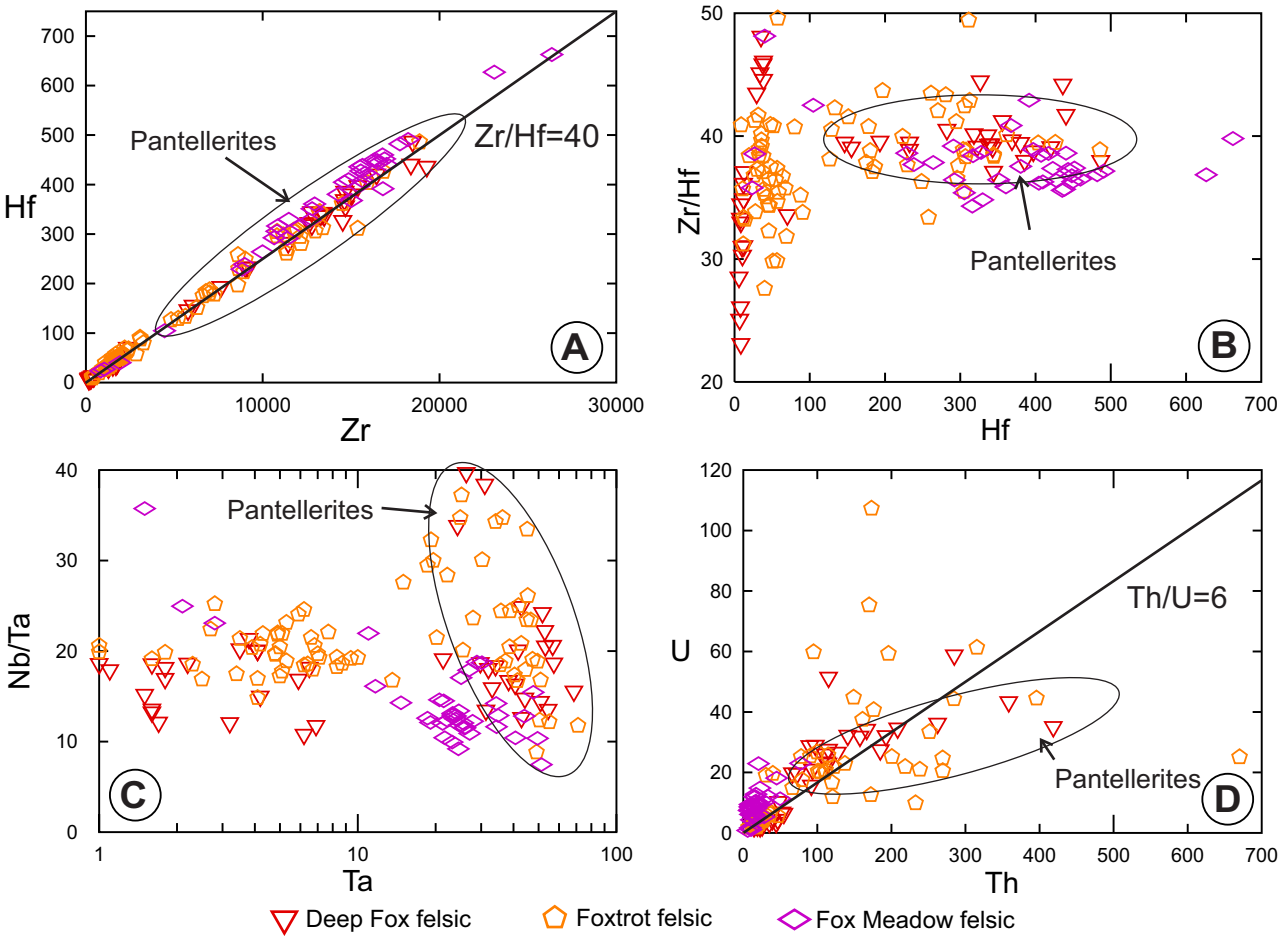

Figure 7. *Trace element correlations in the FHVB. A) Hf* vs. *Zr; B) Zr/Hf* vs. *Hf; C) Nb/Ta* vs. *Ta; D) U* vs. *Th.*

consistent with minimum melt compositions (quartz, K-feldspar and albite), but involve other minerals such as magnetite, pyroxene and calcite (Plate 1); although processes other than partial melting may have caused it (Kretz, 1994). The change in the composition of the felsic rocks from quartz-rich in the east to quartz-poor in the west represents different degrees of fractionation, with the quartz-rich EFHVB being more fractionated (MacDonald, 2012). Although, assimilation of country rocks, which are dominated by granitoids in the east and mafic rocks in the west (Figure 2A), may have also influenced the compositions. The presence of mafic rocks in the WFHVB is also suggested by the occurrence of the medium-grained mafic clasts (Plate 4, samples 060A02 and 355A02).

Mineralogy and textural relationships indicate a complex magmatic evolution. In the pantellerite and pantelleritic trachyte the calcic–sodic pyroxene and amphibole are locally intergrown (Plates 2A and 5A), suggesting that one replaced the other, but the order of crystallization is uncertain. This is common in peralkaline rocks and is due to changes in oxygen fugacity (Dostal *et al.*, 2014; Vasyukova and Williams-Jones, 2018). An increase in the oxygen fugacity, which happens due to cooling of the magma, leads to crystallization of pyroxene, whereas a decrease in oxygen fugacity, which may occur due to an influx of more reduced magma, leads to crystallization of amphibole. The amphibole in the non-peralkaline rhyolite contains less Fe and more Al than the amhibole in the pantellerite consistent with its less peralkaline nature. The non-peralkaline rhyolite also contains less REE minerals, zircon and magnetite than the peralkaline rocks, indicative of its less evolved nature. They also contain more K-feldspar compared to pantellerite, in agreement with peralkaline rocks evolving from metaluminous rocks to more Na-rich and less K-rich compositions due to the “orthoclase effect” (Bailey and Schairer, 1964). The higher magnetite content of the peralkaline rocks is in agreement with their evolution toward a more Fe-rich composition (MacDonald, 2012).

The abundance of calcite and fluorite veins in the felsic rocks suggests the circulation of hydrothermal fluids. Biotite replacing amphibole (Plate 2G, H) is the result of hydrothermal alteration, especially because biotite is not common in

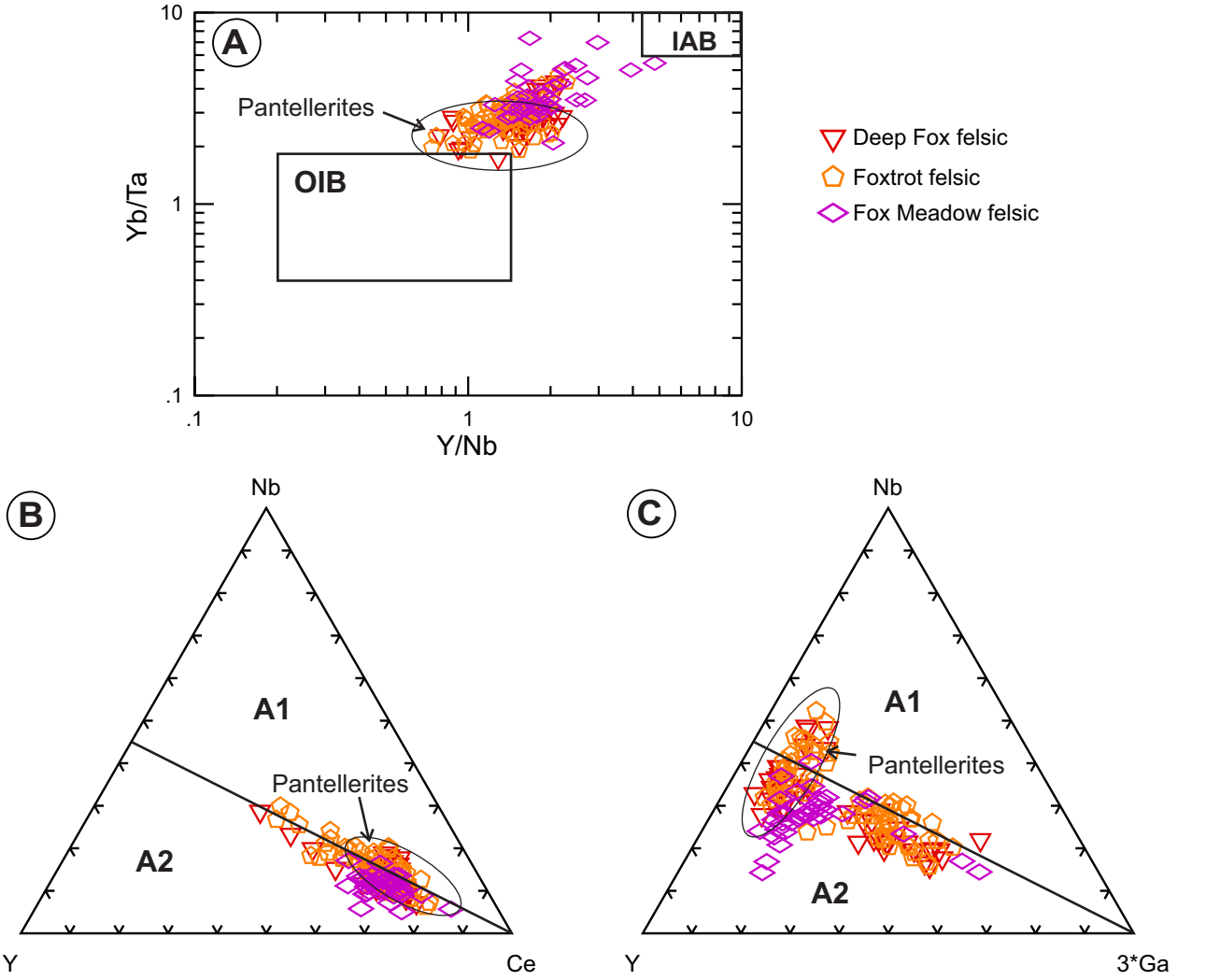

Figure 8. *A) Yb/Ta* vs. *Y/Nb plot (Eby, 1992); B, C) Triangular plots distinguishing the field of A1 and A2 granites (after Eby, 1992).*

pantellerite (MacDonald *et al.*, 2021). Allanite occurring along the cleavage planes of biotite (Plate 5B, C, E) is hydrothermal and zircon in biotite (Plate 5C) may be hydrothermal as well. The effects of metamorphism are uncertain, but the lack of significant lower or higher grade minerals replacing amphiboles is in agreement with amphibolite-facies metamorphism suggested by Haley (2014).

GEOCHRONOLOGY

The ages of comendite and non-peralkaline rhyolite from Deep Fox confirm that they crystallized *ca.* 1.3 Ga, consistent with the ages at the Foxtrot deposit (Haley, 2014) and the other REE-mineralized peralkaline complexes in Labrador (Strange Lake, Red Wine–Letitia Lake, Flowers River; Miller *et al.*, 1997; Crocker, 2014; Ducharme *et al.*, 2021). The zircons in the comendite are also overprinted by a metamorphic age of *ca.* 1.03 Ga. The zircons in pantellerite are slightly smaller and only record a metamorphic age of *ca.* 1.06 Ga. However, based on similarities in mineralogy and whole-rock geochemistry to the comendite and the one zircon core in the pantellerite returning an age of 1238 Ma, igneous crystallization of the pantellerite is interpreted to have also occurred *ca.* 1.3 Ga.

Based on the geochronology results, the comendite is older than the non-peralkaline rhyolite by ~45 Ma, indicating a long magmatic activity, which is consistent with the geochronology results from the Foxtrot area (Haley, 2014). Long-lived and repeatedly reactivated magmatic systems are important for the extensive crystallization required for enrichment of the magma in REEs and associated HFSE, such as Zr, Hf, U and Th (Beard *et al.*, 2022). In most peralkaline igneous complexes the degree of fractionation increases with time (Beard *et al.*, 2022), but the opposite appears to be observed at Deep Fox, where the more

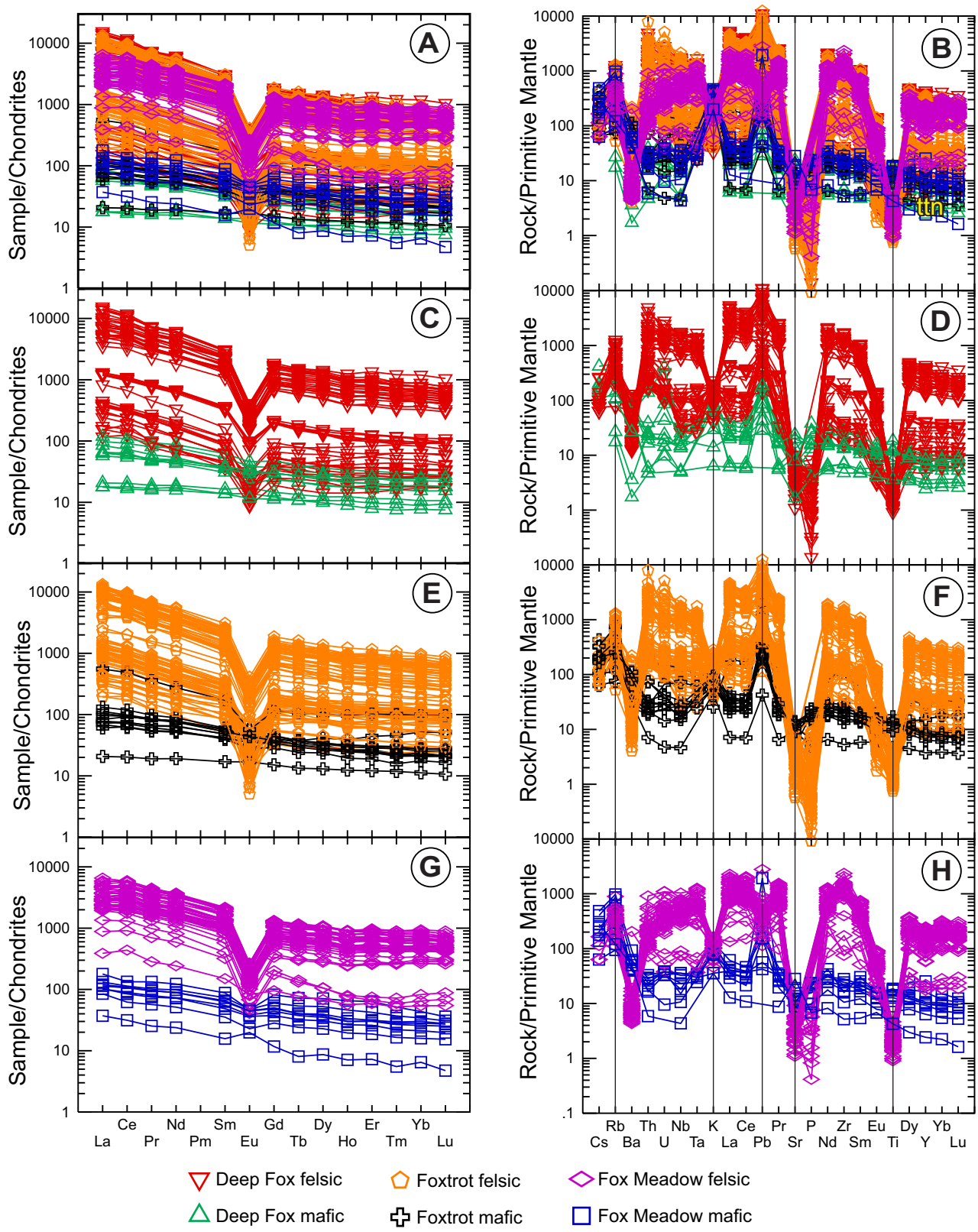

Figure 9. *Chondrite-normalized REE patterns and primitive mantle-normalized plots of the FHVB (Sun and McDonough, 1989). A, B) All samples; C, D) Deep Fox samples; E, F) Foxtrot samples; G, H) Fox Meadow samples. Symbols are the same as in Figure 8.*

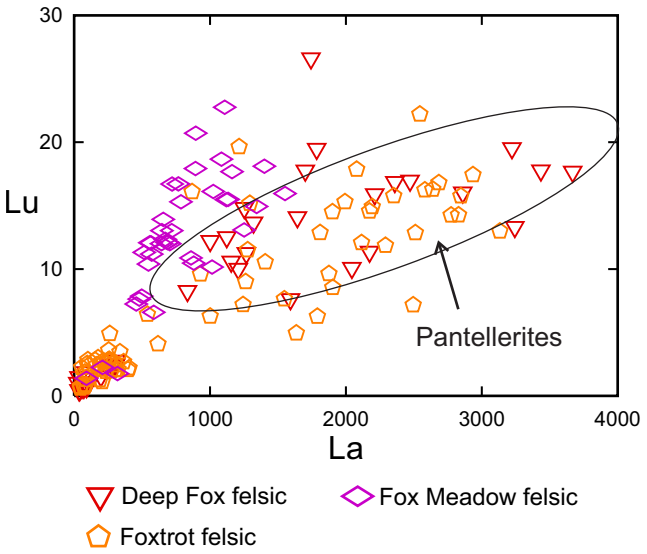

Figure 10. *Lu* vs. *La plot of felsic rocks from the FHVB.*

evolved comendite appears to be older than the less evolved non-peralkaline rhyolite. Possible reasons for this reversal in fractionation trend may be due to tapping a deeper, less evolved portion of the magma chamber or the addition of new, less evolved magma into the magma chamber from below (Civetta *et al.*, 1988). Pantellerite is younger than the non-peralkaline rhyolite based on crosscutting relationships (Plate 7) and the age of crystallization of pantellerite suggested by the one zircon core.

Similar to the pantellerite at Deep Fox, a high-Zr pantellerite from the Road Belt (Haley, 2014) also returned only a metamorphic age, whereas a low-Zr pantellerite from the Road Belt did return an igneous age. The lack of protolith zircons in the two pantellerite samples, despite the presence of adequate Si and Zr, is unusual. One of the reasons for this may be that the strongly mineralized samples were richer in volatiles, with the volatiles also having been enriched during fractionation along with the REEs. Volatile-rich rocks are more susceptible to metamorphism, because they enhance fluid flow and increase rates of crystal growth, diffusion and reaction (Nordlie, 1989).

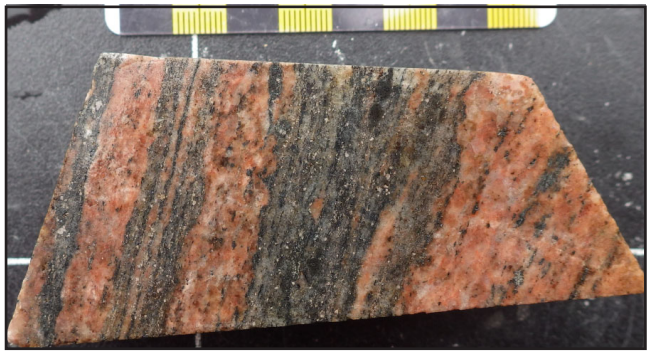

Plate 7. *Pantellerite (dark grey) cutting non-peralkaline rhyolite (pink).*

The leucogabbro, located north of the mineralized rocks at Deep Fox, most likely crystallized *ca.* 1.3 Ga, although it is uncertain due to the limited number of zircons with adequate U content. The connection between the FHVB and the leucogabbro is not clear. The leucogabbro is locally anorthositic and anorthosite (part of the AMCG magmatism) is typically associated with other peralkaline complexes in Labrador. Although, some of these AMCG suites, such as the ~1.4 Ga-old Harp Lake suite, are older than the peralkaline complexes crystallized *ca.* 1.3 Ga (Gower and Krogh, 2002).

GEOCHEMISTRY

Previous studies on the Mesoproterozoic peralkaline complexes associated with REE mineralization in Labrador suggest mantle-derived melts inciting lower crustal melting as the source for these complexes (Gower and Krogh, 2002). The majority of the felsic rocks from the FHVB are A2-type, implying crustal contamination of a most likely mantle-derived magma (Figure 8; Eby, 1990, 1992). Hafnium isotopes in zircon indicate partial melting of 1.9 to 1.5 Ga crustal rocks as the source of the FHVB (Haley, 2014); therefore, the amount of mantle contribution is uncertain and needs further investigation.

The Zr, Hf, Nb and Ta contents of the most evolved rocks indicate a strongly peralkaline melt (Figure 7A–C), despite the apparent metaluminous nature of parts of the FHVB suggested by the major-element concentrations (Figure 5). The solubility of Zr and Hf in the melt strongly depends on the alkalinity (Linnen and Keppler, 2002; Zaraisky *et al.*, 2009), with an increase in the alkalinity resulting in an increase in the solubility of both Zr and Hf. The high Zr content (up to ~26 000 ppm), more than 150 times of the average Zr content of granites (170 ppm; Turekian and Wedepohl, 1961), and high Hf content indicate a strongly peralkaline melt. Although, increase in F content would also increase the solubility of both elements. Increasing Zr/Hf ratios with increasing degree of fractionation and near constant Zr/Hf ratios in the more fractionated rocks are also typical of peralkaline rocks and is due to lack of significant fractionation of Zr and Hf during crystallization of zircon in peralkaline melts (Linnen and Keppler, 2002). Similar to the Zr/Hf ratio, variations in the Nb/Ta ratios are also typical of peralkaline rocks, showing no negative correlation with increasing Ta content (Linnen and Keppler, 1997). This is due to the dependence of the solubilities of minerals containing Nb and Ta (*e.g.*, rutile) on the peralkalinity of the melt. The reason for the apparent metaluminous nature of parts of the FHVB is hydrothermal alter-

ation that resulted in K-metasomatism and Na-loss (Figure 6; Hughes, 1973; Spitz and Darling, 1978), which is consistent with amphibole being partially altered to biotite observed in some samples (Plate 2G, H). Sodium loss has been documented in other peralkaline complexes, such as Strange Lake, Flowers River and the St. Lawrence Granite (Miller, 1994; Vasyukova and Williams-Jones, 2018; Magyarosi, 2022), and is attributed to the breakdown of sodic amphiboles and feldspars due to the presence of late-magmatic fluids rich in F, C and Cl altering the rocks. At FHVB, the presence of similar fluids is indicated by the abundance of calcite and fluorite veins, although subsequent Grenvillian metamorphism may have also altered the rocks. All pantellerites were affected (Figure 6) probably due to their higher initial volatile content, which increases with increasing degree of fractionation along with the REEs and HFSE. Sodium depletion at Flowers River was associated with a volcanic phase accompanied by high levels of hydrothermal activity, most likely due to higher volatile content, and also affected the most evolved volcanic rocks (Zr > 5000 ppm, Al_2O_3 < 10.5 wt. %; Miller, 1994).

The HHP nature of most of the FHVB, indicated by its high Th and U contents and Th/U ratio, implies that the rocks cooled slower than regular granitic rocks. This allowed more time for fractionation and was able to sustain the circulation of late-magmatic fluids for a longer time than in regular granitic rocks; both of these processes were essential for the strong enrichment in REEs.

Chondrite-normalized plots of the felsic rocks are typical of A-type granites having a negative slope from La to Lu and a deep negative Eu anomaly, and indicate the strong enrichment in REEs (Figure 8). The reasons for the EFHVB being overall richer in both LREE and HREE and the higher HREE/LREE ratio in the WFHVB are uncertain (Figure 9). Primitive mantle-normalized plots indicate fractionation of feldspars and other minerals (possibly titanite, apatite), also typical of A-type granites (Figure 8).

REE MINERALIZATION

Most of the REE minerals crystallized late, indicated by their textural relationships. Some of the allanite was likely magmatic, suggested by its spatial association with other magmatic phases such as zircon, magnetite and titanite, and the lack of textures indicating that allanite replaced another primary REE mineral. Although some zircon clearly crystallized during metamorphism, others may be hydrothermal. Allanite occurring as veins and in the cleavage planes of biotite, formed as alteration after amphibole, is likely hydrothermal. Changes in the composition of allanite may have been due to magmatic, hydrothermal and metamorphic processes. Fergusonite is most commonly spatially associated with zircon, occurring around the crystal boundaries of the zircon grains. The reason for the occurrence of galena in fergusonite is uncertain. Galena may have formed earlier or Pb was remobilized later; the latter is suggested by the occurrence of amazonite in and around pegmatites, most likely formed during later metamorphism, although its textural relationship with fergusonite suggests that galena crystallized first (Plate 2E). Rare-earth-element-rich titanite only occurs in the WFHVB where it crystallized before allanite, suggesting a magmatic origin.

A significant difference between the various REE-mineralized peralkaline complexes in Labrador is the depth of the intrusions, which has a great effect on the REE mineralization (Beard *et al.*, 2022). Peralkaline volcanic-hosted REE mineralization is less common than intrusive-hosted mineralization, related to the dependence of the behaviour of volatiles on the depth of the intrusion (Beard *et al.*, 2022). Due to their fluxing nature, volatiles are important for extended fractional crystallization leading to REE mineralization, and volcanic rocks may not be able to retain the volatiles due to their shallow depth. However, according to MacDonald *et al.* (2021), F contents of peralkaline rhyolites range up to 2.2 wt. %, arguing against complete devolatilization. The high F content of the FHVB (up to 7346 ppm), and the abundance of fluorite, calcite and apatite contradict the loss of volatiles. In addition, most of the fractionation leading to REE enrichment is postulated to have happened in a magma chamber prior to the intrusion of the volcanic rocks above (Beard *et al.*, 2022).

SUMMARY

- The FHVB crystallized *ca.* 1.3 Ga, similar to the other REE-mineralized peralkaline complexes in Labrador, and went through metamorphism and deformation during Grenville orogeny *ca.* 1.05 Ga.

- Chemistry of FHVB and Hf isotopes in zircon suggest significant crustal contamination for the FHVB (Haley, 2014). The amount of mantle contribution is uncertain.

- The extent of the FHVB is uncertain: the ages of rocks separating the mineralized belts and the rocks to the south hosting REE occurrences are unknown.

- The FHVB is bimodal and the felsic rocks are quartz-saturated peralkaline to metaluminous volcanic rocks, with the quartz content decreasing from east to west.

- The evolution of the FHVB and associated REE mineralization is the result of magmatic, late-magmatic hydrothermal and metamorphic processes.

- Magmatic evolution is typical of peralkaline igneous systems: changes in oxygen fugacity, decreasing K-feldspar content (orthoclase effect) and increasing Fe, REEs, HFSE and volatile contents with increasing degree of fractionation.

- Pantellerite is the youngest felsic rock consistent with increasing degree of fractionation with time, but non-peralkaline rhyolite is younger than the more evolved comendite, contrary to this trend.

- Both Na and K were remobilized by late-magmatic hydrothermal fluids, common in peralkaline igneous systems, resulting in the apparent metaluminous nature of parts of the FHVB, including the most evolved pantellerites.

- The main REE minerals include allanite, fergusonite and REE–titanite, differing from the REE mineralogy in the other peralkaline complexes in Labrador (Hill, 1982; Miller *et al.*, 1997; Kerr, 2011, 2015; Crocker, 2014; Ducharme *et al.*, 2021).

- Typical hydrothermal REE minerals are rare, but some of the allanite and possibly zircon are hydrothermal.

- Mineral assemblages are consistent with amphibolite-grade metamorphism indicated by Haley (2014).

- Pantellerite returned only a metamorphic age suggesting that it was more susceptible to metamorphism possibly due to its higher volatile content.

- The FHVB is HHP, which allowed more time for fractionation and circulation of late-magmatic hydrothermal fluids, both processes essential for REE mineralization.

FURTHER STUDIES

This report presents a significant amount of new data on the FHVB and associated REE mineralization, but also highlights our lack of understanding of this type of deposit and the need for more research to understand the various processes leading to REE mineralization at FHVB. Additional whole-rock geochemistry, geochronology and mineralogy along the FHVB will examine variations in the rock types, REE concentrations and relationships between the occurrences and the three mineralized belts. This work will include the rocks separating the three mineralized belts to determine the spatial extent of the FHVB, which is under debate (Miller, 2015; Gower, 2019). The occurrences located south of the FHVB in the Pinware terrane, and their host rocks, will also be examined to determine the relationship, if any, between the FHVB and these occurrences. Further SEM and EPMA analyses will be undertaken to identify all minerals, modal mineralogy, mineral chemistry of the REE minerals and the main silicates, textural features, mineral associations and any zoning to distinguish the various processes leading to REE mineralization. Detailed geochronology and trace-element chemistry of minerals, such as zircon and allanite, occurring in all areas would also help in identifying and distinguishing all these processes. Neodymium and Sm isotopes will shed light on the origin of the rocks (*e.g.*, mantle *vs.* crustal). A detailed structural study is currently being undertaken to examine the effects of deformation on the host and surrounding rocks, and REE mineralization.

ACKNOWLEDGMENTS

This paper is a contribution to Natural Resources Canada's (NRCan) TGI Program of the GSC. Support for this study was provided through the Magmatic Ore Systems Project's 'Sub-Activity: Critical minerals within carbonatite, syenite, and allied peralkaline-alkaline rocks in the central and eastern parts of the Canadian Shield: where, when and how were they formed' and by the GSNL. Lindsay Oldham and Arianna Sheppard are thanked for their assistance during fieldwork in the summers of 2021 and 2022. Gerry Hickey helped with providing some of the equipment for and after the fieldwork. Joanne Rooney and Kim Morgan are acknowledged for typesetting and figure preparation, respectively. ZM is grateful to Randy Miller and the crew from Search Minerals Incorporated for their tremendous help during both field seasons. John Hinchey is thanked for his support in every aspect of the work. Anne-Aurélie Sappin from the GSC and Dave Corrigan, formerly from the GSC, are thanked for their liaison with the GSC. Dylan Goudie provided his assistance with the SEM and SEM-MLA analyses. NR is grateful for the support and assistance of the staff of the Geochronology Laboratories of the Geological Survey of Canada. In particular, Ray Chung, Greg Case and Tom Pestaj are thanked for their careful efforts and excellent work. Matt Polivchuk provided the necessary high-quality scanning electron microscope images. ZM is grateful for the discussions with Dr. Eric Thiessen and Nicolas Prieto Moreno about the geology of the study area and is looking forward to the results of their structural study. This is Natural Resources Canada Contribution Number 20220619.

REFERENCES

Bailey, D.K. and Schairer, J.F.
1964: Feldspar-liquid equilibria in peralkaline liquids – The orthoclase effect. American Journal of Science, Volume 262, pages 1198-1206.

Beard, C.D., Goodenough, K.M., Borst, A.M., Wall, F., Siegfried, P.R., Deady, E.A., Pohl, C., Hutchison, W., Finch, A.A., Walter, B.F., Elliott, H.A.L. and Brauch, K.
2022: Alkaline-silicate REE-HFSE systems. Economic Geology, Volume 118, pages 177-208.

Black, L.P., Kamo, S.L., Allen, C.M., Davis, D.W., Aleinikoff, J.N., Valley, J.W., Mundil, R., Campbell, I.H., Korsh, R.J., Williams, I.S. and Foudoulis, C.
2004: Improved $^{206}Pb/^{238}U$ microprobe geochronology by monitoring of a trace-element-related matrix effect; SHRIMP, ID-TIMS, ELA-ICP-MS and oxygen isotope documentation for a series of zircon standards. Chemical Geology, Volume 205, pages 115-140.

Bodorkos, S., Bowring, J. and Rayner, N.
2020: Squid3: Next-generation data processing software for Sensitive High Resolution Ion Micro Probe (SHRIMP). Exploring for the Future: Abstracts. Geoscience Australia.

Christiansen, E.H. and Keith, J.D.
1996. Trace element systematics in silicic magmas: a metallogenic perspective. *In* Trace Element Geochemistry of Volcanic Rocks: Applications for Massive Sulphide Exploration. *Edited by* D.A. Wyman. Geological Association of Canada, Short Course Notes, Volume 12, pages 115-151.

Ciuculescu, T., Masun, K.M., Weir, I., Vasquez, L. and Goode, J.R.
2022: Technical report on the Deep Fox and Foxtrot Project, Newfoundland and Labrador, Canada. NI 43-101 for Search Minerals Inc., SLR Consulting (Canada) Ltd., 281 pages.

Civetta, L., Cornette, Y., Gillot, P.Y. and Orsi, G.
1988: The eruptive history of Pantelleria (Sicily Channel) in the last 50 ka. Bulletin of Volcanology, Volume 50, pages 47-57.

Crocker, M.G.
2014: A petrographic, geochemical and geochronological study of rare earth mineralization in the Red Wine Intrusive Suite, Labrador, Canada. Unpublished M.Sc. thesis, Memorial University of Newfoundland, 766 pages.

Davis, W.J., Pestaj, T., Rayner, N. and McNicoll, V.M.
2019: Long-term reproducibility of $^{207}Pb/^{206}Pb$ age at the GSC SHRIMP lab based on the GSC Archean reference zircon z1242. Geological Survey of Canada, Scientific Presentation 111, 1 poster.

Dostal, J.
2016: Rare metal deposits associated with alkaline/peralkaline igneous rocks. Reviews in Economic Geology, Volume 18, pages 33-54.

Dostal, J., Kontak, D.J. and Karl, S.M.
2014: The Early Jurassic Bokan Mountain peralkaline granitic complex (southeastern Alaska): Geochemistry, petrogenesis and rare-metal mineralization. Lithos, Volume 202-203, pages 395-412.

Ducharme, T.A., McFarlane, C.R.M., van Rooyen, D. and Corrigan, D.
2021: Petrogenesis of the peralkaline Flowers River Igneous Suite and its significance to the development of the southern Nain Batholith. Geological Magazine, Volume 168, pages 1911-1936.

Eby, G.N.
1990: The A-type granitoids: A review of their occurrence and chemical characteristics and speculations on their petrogenesis. Lithos, Volume 26, pages 115-134.

1992: Chemical subdivision of the A-type granitoids: petrogenetic and tectonic implications. Geology, Volume 20, pages 641-644.

Finch, C., Roldan, R., Walsh, L., Kelly, J. and Amor, S.
2018: Analytical methods for chemical analysis of geological materials. Government of Newfoundland and Labrador, Department of Natural Resources, Geological Survey, Open File NFLD/3316, 67 pages.

Förster, H.-J., Tischendorf, G. and Trumbull, R.B.
1997: An evaluation of the Rb *vs.* (Y +Nb) discrimination diagram to infer tectonic setting of silicic igneous rocks. Lithos, Volume 40, pages 261-293.

Goode, J.R.
2021: The extractive metallurgy of rare earth elements. PEGNL Professional Short Course: Critical Minerals and Net Zero. Presentation at Mineral Resources Review, CIM NL Branch, St. John's.

Gower, C.F.
2010a: Bedrock geological maps for the Grenville Province and adjacent Makkovik Province in eastern Labrador. Government of Newfoundland and Labrador, Department of Natural Resources, Geological Survey, Maps 2010-01 to 2010-25, 1:100 000 scale.

2010b: Geology of the Grenville Province and adjacent eastern Makkovik Province, eastern Labrador.

Geological Survey of Newfoundland and Labrador, Map 2010-50, scale 1:500 000.

2019: Regional geology of eastern Labrador (eastern Makkovik and Grenville provinces). Government of Newfoundland and Labrador, Department of Natural Resources, Geological Survey, Memoir 4, 654 pages.

Gower, C.F. and Krogh, T.E.
2002: A U–Pb geochronological review of the Proterozoic history of the eastern Grenville Province. Canadian Journal of Earth Sciences, Volume 39, pages 795-829.

Haley, J.T.
2014: 1.3 Ga bimodal volcanism in southeastern Labrador: Fox Harbour. Unpublished M.Sc. thesis, Memorial University of Newfoundland, St. John's, Newfoundland, 209 pages.

Hill, J.
1982: Geology of the Flowers River–Notokwanon River area, Labrador. Government of Newfoundland and Labrador, Department of Mines and Energy, Mineral Development Division, Report 82-6, 140 pages.

Hughes, C.J.
1973: Spilites, keratophyres, and the igneous spectrum. Geological Magazine, Volume 109, pages 513-527.

Kerr, A.
2011: Rare-rarth element (REE) mineralization in Labrador: A review of known environments and the geological context of current exploration activity. *In* Current Research. Government of Newfoundland and Labrador, Department of Natural Resources, Geological Survey, Report 11-1, pages 109-145.

2015: Sm-Nd isotopic geochemistry of rare-earth-element (REE) mineralization and associated peralkaline granites of the Strange Lake intrusion, Labrador. *In* Current Research. Government of Newfoundland and Labrador, Department of Natural Resources, Geological Survey, Report 15-1, pages 63-83.

Kretz, R.
1994: Metamorphic crystallization. John Wiley & Sons Ltd., 520 pages.

Linnen, R.L. and Keppler, H.
1997: Columbite solubility in granitic melts: consequences for the enrichment and fractionation of Nb and Ta in the Earth's crust. Contributions to Mineralogy and Petrology, Volume 128, pages 213-227.

2002: Melt composition control of Zr/Hf fractionation in magmatic processes. Geochimica et Cosmochimica Acta, Volume 66, pages 3293-3301.

Ludwig, K.
2012. User's manual for Isoplot/Ex rev. 3.70: A Geochronological Toolkit for Microsoft Excel. Special Publication, 5, Berkeley Geochronology Center, Berkeley, 76 pages.

MacDonald, R.
1974: Nomenclature and petrochemistry of the peralkaline oversaturated extrusive rocks. Bulletin Volcanologique, Volume 38, pages 498-516.

2012: Evolution of peralkaline silicic complexes: Lessons from the extrusive rocks. Lithos, Volume 152, pages 11-22.

MacDonald, R., White, J.C. and Belkin, H.E.
2021: Peralkaline silicic extrusive rocks: magma genesis, evolution, plumbing systems and eruption. Compte Rendus Géoscience, Science de la Planète, Volume 353, Special Issue S2, pages 7-59.

Magyarosi, Z.
2022: Late-magmatic processes in the St. Lawrence Granite: Implications for fluorite mineralization. Journal of Geochemical Exploration, Volume 239. Article 107014

Masun, K.M., Weir, I.C. and Goode, J.R.
2016: Technical report on the Foxtrot project, Newfoundland and Labrador, Canada. NI 43-101 report for Search Minerals Inc., Roscoe Postle Associates Inc., 219 pages.

Miller, R.R.
1994: Extreme Na-depletion in the peralkaline volcanic rocks of the middle Proterozoic Flowers River cauldron complex, Labrador. *In* Current Research. Government of Newfoundland and Labrador, Department of Mines and Energy, Geological Survey Branch, Report 94-1, pages 233-246.

2015: Pantellerite-hosted rare earth element mineralization in southeast Labrador: The Foxtrot deposit. *In* Symposium on Strategic and Critical Materials Proceedings. *Edited by* G.J. Simandl and M. Neetz. British Columbia Ministry of Energy and Mines, British

Columbia Geological Survey, Paper 2015-3, pages 109-117.

Miller, R.R., Heaman, L.M. and Birkett, T.C.
1997: U-Pb zircon age of the Strange Lake peralkaline complex: Implications for Mesoproterozoic peralkaline magmatism in north-central Labrador. Precambrian Research, Volume 81, pages 67-82.

Nordlie, B.E.
1989: Volatiles. *In* Petrology, Encyclopedia of Earth Science, Springer, Boston, MA, pages 597-599.

Nunn, G.A.G. and van Nostrand, T.
1996a: Geology of the Kenemich River map area (NTS 13G/SW), Labrador. *In* Current Research. Government of Newfoundland and Labrador, Department of Natural Resources, Geological Survey, Report 96-1, pages 73-83.

1996b: Geology of the Kenemich River map area, Labrador. Map 96-34. Government of Newfoundland and Labrador, Department of Natural Resources, Geological Survey, Open File 13G/0048.

Pearce, J.A.
1996: A user's guide to basalt discrimination diagrams. *In* Trace Element Geochemistry of Volcanic Rocks: Applications for Massive Sulphide Exploration. *Edited by* D.A. Wyman. Geological Association of Canada, Short Course Notes, Volume 12, pages 79-113.

Pearce, J.A., Harris, N.B.W. and Tindle, A.G.
1984: Trace element discrimination diagrams for the tectonic interpretation of granitic rocks. Journal of Petrology, Volume 25, pages 956-983.

Shand, S.J.
1922: The problem of the alkaline rocks. *In* Proceedings of the Geological Society of South Africa, Volume 25, pages 19-33.

Sharma, R., Kumar, N. and Kumar N..
2019: Signatures of high heat production and mineralization associated with plutonic and volcanic acidic rocks from Tosham Ring Complex, Southwestern Haryana, India. Himalayan Geology, Volume 40, pages 239-247.

Spitz, G. and Darling, R.
1978: Major and minor element lithogeochemical anomalies surrounding the Louvem copper deposit, Val d'Or, Quebec. Canadian Journal of Earth Sciences, Volume 15, pages 1161-1169.

Steiger, R.H. and Jäger, E.
1977: Subcommission on geochronology; convention on the use of decay constants in geo- and cosmochronology. Earth and Planetary Science Letters, Volume 36, pages 359-362.

Stern, R.A.
1997: The GSC Sensitive High Resolution Ion Microprobe (SHRIMP): Analytical techniques of zircon U-Th-Pb age determinations and performance evaluation. *In* Radiogenic Age and Isotopic Studies: Report 10. Geological Survey of Canada, Current Resarch 1997-F, pages 1-31.

Stern, R.A. and Amelin, Y.
2003. Assessment of errors in SIMS zircon U-Pb geochronology using a natural zircon standard and NIST SRM 610 glass. Chemical Geology, Volume 197, pages 111-146.

Sun, S.S. and McDonough, W.F.
1989. Chemical and isotopic systematics of oceanic basalts: implications for mantle composition and processes. *In* Magmatism in the Ocean Basins. *Edited by* A.D. Saunders and M.J. Norry. Geological Society of London, Special Publication 42, pages 313-345.

Turekian, K.L. and Wedepohl, K.H.
1961: Distribution of elements in some major units of the Earth's crust. Geological Society of America Bulletin, Volume 72, pages 175-192.

van Nostrand, T.
1992: Geology of the Alexis River region, Grenville Province, southeastern Labrador. Government of Newfoundland and Labrador, Department of Mines and Energy, Report 92-3, 27 pages.

van Nostrand, T., Dunphy, D. and Eddy, D.
1992: Geology of the Alexis River region, Grenville Province, southeastern Labrador. *In* Current Research. Government of Newfoundland and Labrador, Department of Mines and Energy, Geological Survey Branch, Report 92-1, pages 399-412.

Vasyukova, O.E. and Williams-Jones, A.E.
2018: Direct measurement of metal concentrations in fluid inclusions, a tale of hydrothermal alteration and REE ore formation from Strange Lake, Canada. Chemical Geology, Volume 483, pages 385-396.

Wardle, R.J., Gower, C.F., Ryan, B., Nunn, G.A.G., James, D.T. and Kerr, A.
1997: Geological map of Labrador; 1:1 million scale.

Government of Newfoundland and Labrador, Department of Mines and Energy, Geological Survey, Map 97-07.

Whalen, J.B., Currie, K.L. and Chappell, B.W.
1987: A-type granites: geochemical characteristics, discrimination and petrogenesis. Contributions to Mineralogy and Petrology, Volume 95, pages 407-419.

Whitney, D.L.
2010: Abbreviations for names of rock-forming minerals. American Mineralogist, Volume 95, pages 185-187.

Zaraisky, G.P., Aksyuk, A.M., Devyatova, V.N., Udoratina, O.V. and Chevychelov, V.Y.
2009: The Zr/Hf ratio as a fractionation indicator of rare-metal granites. Petrology, Volume 17, pages 25-45.